Cellular and Molecular Life Sciences (2025) 82:149
https://doi.org/10.1007/s00018-025-05684-y

ORIGINAL ARTICLE

Circular RNA circSTX12 regulates osteo-adipogenic balance and proliferation of BMSCs in senile osteoporosis

Huimin Gu[1,3] · Wenhui Yu[2,3] · Pei Feng[1,3] · Chenying Zeng[1,3] · Qian Cao[1,3] · Fenglei Chen[2,3] · Ziming Wang[2,3] · Huiyong Shen[2,3] · Yanfeng Wu[1,3] · Shan Wang[1,3]

Received: 20 June 2024 / Revised: 3 January 2025 / Accepted: 28 March 2025

Abstract

Increased adipogenic differentiation and decreased osteogenic differentiation of bone marrow mesenchymal stem cells (BMSCs) along with slow self-renewal are pivotal causes for decreased bone formation in senile osteoporosis. Circular RNAs (circRNAs) play important roles in cell proliferation and differentiation, and are closely related to osteoporosis. Whether circRNAs orchestrate the adipo-osteogenic balance and the proliferation of BMSCs in osteoporosis remains unclear. We found in this study that circSTX12 was abnormally upregulated in bone sections from osteoporosis patients and in BMSCs from aged mice, as well as in later-generation human BMSCs in culture. Knockdown of circSTX12 in BMSCs resulted in enhanced osteogenesis, decreased adipogenesis, and increased proliferation capacity; circSTX12 overexpression had the opposite effect. RNA pull-down and mass spectrometry revealed the interactions between circSTX12 with CBL and LMO7. At the molecular level, circSTX12 regulated cell fate in BMSCs by competitively binding to CBL, reducing the ubiquitination-mediated degradation of MST1 and thereby activating the Hippo pathway, a key regulator of adipo-osteogenic balance. Knockdown of circSTX12 promoted the nuclear localization of YAP. In addition, our findings suggest that LMO7 mediates circSTX12-induced BMSCs proliferation by regulating the transcription of CCNA2, CCNH, and CCND1. In vivo, injection of antisense oligonucleotides (ASOs) to knockdown circSTX12 promoted bone formation in aged mice. Our results provide evidence for circSTX12 as a regulator of adipo-osteogenic differentiation and proliferation of BMSCs through binding to CBL and LMO7, respectively. Targeting circSTX12 may be a novel approach for osteoporosis treatment.

Huimin Gu, Wenhui Yu and Pei Feng contributed equally to this work.

✉ Huiyong Shen
shenhuiy@mail.sysu.edu.cn

✉ Yanfeng Wu
wuyf@mail.sysu.edu.cn

✉ Shan Wang
wangsh245@mail.sysu.edu.cn

[1] Center for Biotherapy, Eighth Affiliated Hospital of Sun Yat-sen University, Shenzhen 518033, P. R. China

[2] Department of Orthopedics, Eighth Affiliated Hospital of Sun Yat-sen University, Shenzhen 518033, P. R. China

[3] Guangdong Provincial Clinical Research Center for Orthopedic Diseases, The Eighth Affiliated Hospital of Sun Yat-sen University, Shenzhen 518033, P. R. China

Published online: 07 April 2025

Graphical abstract

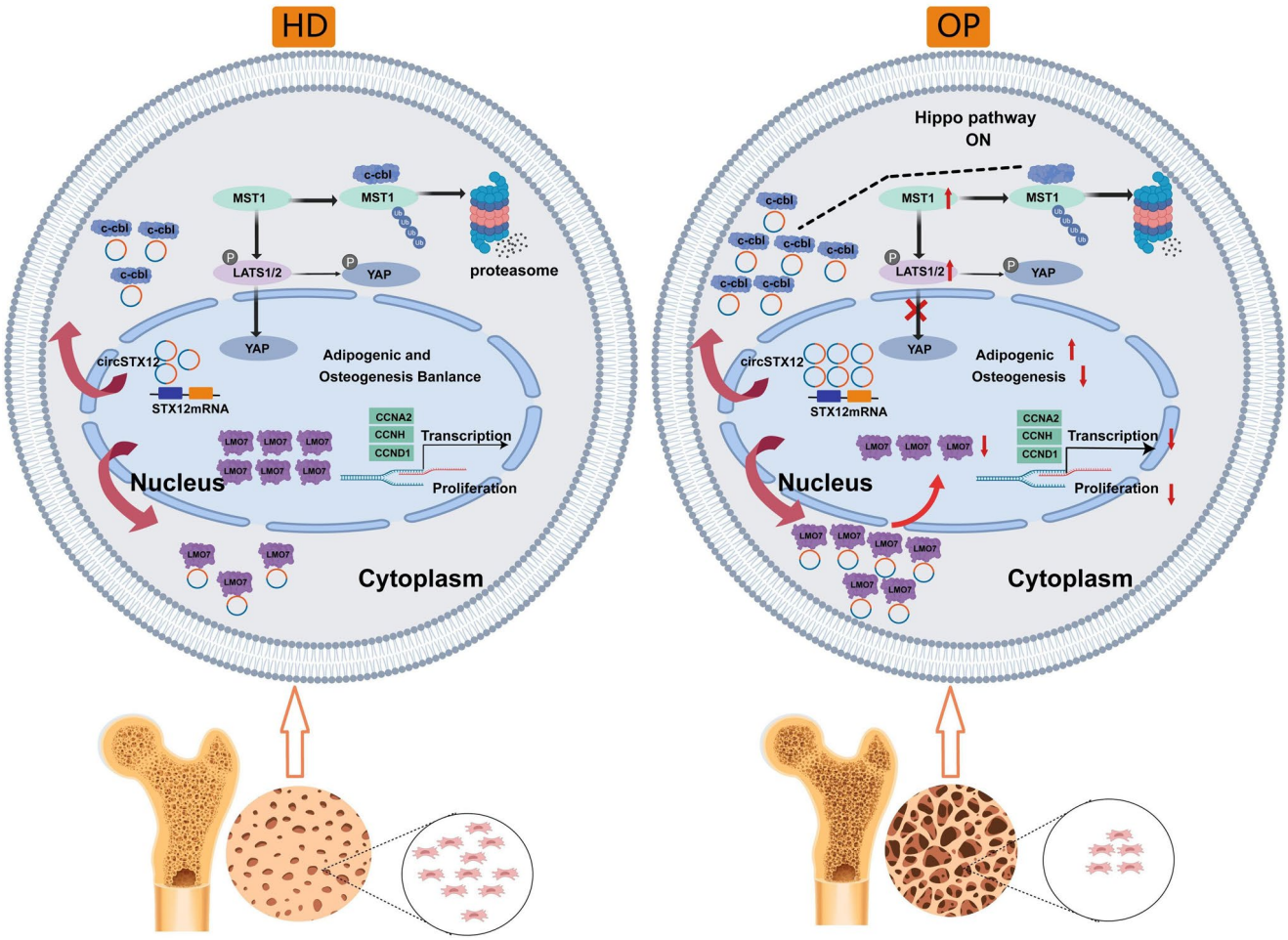

Keywords Senile osteoporosis · Bone marrow mesenchymal stem cells · circSTX12 · CBL · LMO7

Abbreviations

circular RNAs	circRNAs
AS	Ankylosing spondylitis
OP	Osteoporosis
BMSCs	Bone marrow mesenchymal stem cells
HDs	Healthy donors
KEGG	Kyoto Encyclopedia of Genes and Genomes
GO	Gene Ontology
CBL	Cbl proto-oncogene
LMO7	LIM domain 7
OCN	Bone Gamma-carboxyglutamate protein
RUNX2	RUNX family transcription factor 2
OSX	Sp7 Transcription factor
OPN	Secreted phosphoprotein 1
STX12	Syntaxin 12
PPARG	Peroxisome proliferator activated receptor gamma
FABP4	Fatty acid binding protein 4
CEBPA	CCAAT enhancer binding protein alpha
AKT1	AKT serine/threonine kinase 1
Wnt1	Wnt family member 1
BMP2	Bone morphogenetic protein 2
Gli1	GLI FAMILY zinc finger 1
LATS1	Large tumour suppressor kinase 1
MST1	Macrophage stimulating 1
YAP	Yes1-associated transcriptional regulator
H3	Histone 3
CCNA2	Cyclin A2
CCNH	Cyclin H
CCND1	Cyclin D1
ASO	Antisense oligonucleotide
siRNAs	small-interfering RNAs

Introduction

Senile osteoporosis (OP), a disease of skeletal metabolism, is characterized by reduced bone mass and deterioration of the microstructure of the bone tissue and is associated with increased fracture risk. As the population ages, the individual and societal costs of senile osteoporosis are increasing annually, posing a challenge to public health [1]. The balance of bone reconstruction and resorption maintains skeletal homeostasis. Increased bone resorption and decreased bone reconstruction are two pivotal causes of the development of senile osteoporosis. Both genetic and environmental factors influence the development of senile osteoporosis by interfering with the differentiation and activity of osteoblasts and osteoclasts, which mediate bone reconstruction and resorption, respectively [2]. Bone marrow mesenchymal stem cells (BMSCs), which are adult stem cells that undergo multidirectional differentiation and self-renewal, are important sources of osteoblasts [3]. The transition of osteoblasts to adipocytes, coupled with the decreased proliferation capacity of BMSCs, are important causes of osteoporosis during ageing [4]. The choice of osteogenic or adipogenic commitment and proliferation of BMSCs are controlled by several crucial factors. For example, PPARγ and CEBPα/β/δ are master regulators of adipocyte differentiation [5], while RUNX2 and SP7 constitute essential cascades for the osteoblast program [6, 7]. Cyclin-dependent kinases (CDKs), cyclins, and CDK inhibitors (CKIs) are crucial factors of cell proliferation [8]. However, further research for the molecular network orchestrating the adipo-osteogenic balance and proliferation of BMSCs in senile osteoporosis is still needed.

Epigenetic modifications, including DNA methylation, histone modifications, and RNA-based mechanisms regulate gene expression without changing the underlying DNA sequence [6, 9–11]. As a multifactorial disease, senile osteoporosis is strongly influenced by epigenetic factors [11]. Circular RNAs (circRNAs) are a large class of circular closed single-stranded RNAs that are produced by reverse splicing. Due to the lack of a 5'-end cap and 3'-end tail structure, they can withstand digestion by endonucleases and are more stable than linear mRNAs [12]. Due to their high stability, circRNAs can accumulate in specific cell and tissue types [13]. With the development of epigenetic research, increasing evidence has shown that circRNAs are closely related to the occurrence and development of various diseases, including inflammatory diseases, metabolic diseases and cancer [14]. Several circRNAs have been reported to play roles in BMSCs differentiation and may be potential biomarkers for osteoporosis [15, 16]. CircRNA-vgll3 promotes osteogenic differentiation via modulating miRNA-dependent integrinα5 expression [17]. Circ_0024097 originated from YAP activates Wnt/β-catenin pathway to attenuate osteoporosis [18]. However, there are still relatively few studies on circRNAs compared to miRNAs and lncRNAs [19]. Moreover, most of the current studies are limited to the analysis of circRNA microarrays and other expression profile data [20]. A few mechanistic studies have focused mainly on circRNAs as miRNA sponges regulating biological processes [6, 21]. However, the functions of circRNAs are diverse, including effects on protein binding, ribosomal translation and transcriptional regulation [22], which are worthy of further study in the context of osteoporosis.

CircSTX12, with a length of 170nt, is sequenced in our previous work [23]. Here we found that circSTX12 is abnormally upregulated in bone sections from senile osteoporosis patients and in BMSCs from aged mice, as well as in later generations of human BMSCs in culture. Knockdown of circSTX12 in BMSCs resulted in enhanced osteogenesis, decreased adipogenesis, and increased proliferation capacity, while circSTX12 overexpression had the opposite effect. Mechanistically, circSTX12 competitively bound to CBL, leading to reduced ubiquitination and degradation of MST1 and subsequently activating the Hippo pathway, inhibiting YAP nuclear translocation and ultimately promoting the adipogenic differentiation and alleviating the osteogenic differentiation of BMSCs. Additionally, circSTX12 sequesters LMO7 in the cytoplasm, reducing the transcription of CCNA2, CCNH, and CCND1, eventually inhibiting BMSCs proliferation. Knockdown of circStx12 expression with antisense oligonucleotides (ASOs) promoted bone formation in aged mice. Collectively, our findings highlight the involvement of circSTX12 in modulating the differentiation and proliferation of BMSCs, making it a promising therapeutic target for the treatment of senile osteoporosis.

Results

Characteristics of circSTX12

Circularization of human STX12 exon 2 and exon 3 results in the formation of hsa_circ_0008126, named circSTX12 in this manuscript. We first designed divergent primers and used qPCR to test circSTX12 expression in BMSCs. The RT-qPCR-amplified products were subjected to Sanger sequencing, and the presence of the back-splice junction site between exon 3 and exon 2 of STX12 was confirmed (Fig. 1A). Moreover, circSTX12 could be amplified by divergent primers from cDNA but not from gDNA (Fig. 1B). In addition, circSTX12 was resistant to RNase R, whereas the STX12 mRNA level decreased significantly after RNase R treatment (Fig. 1C and D). Next, the localization of circSTX12 was analysed by subcellular fractionation followed

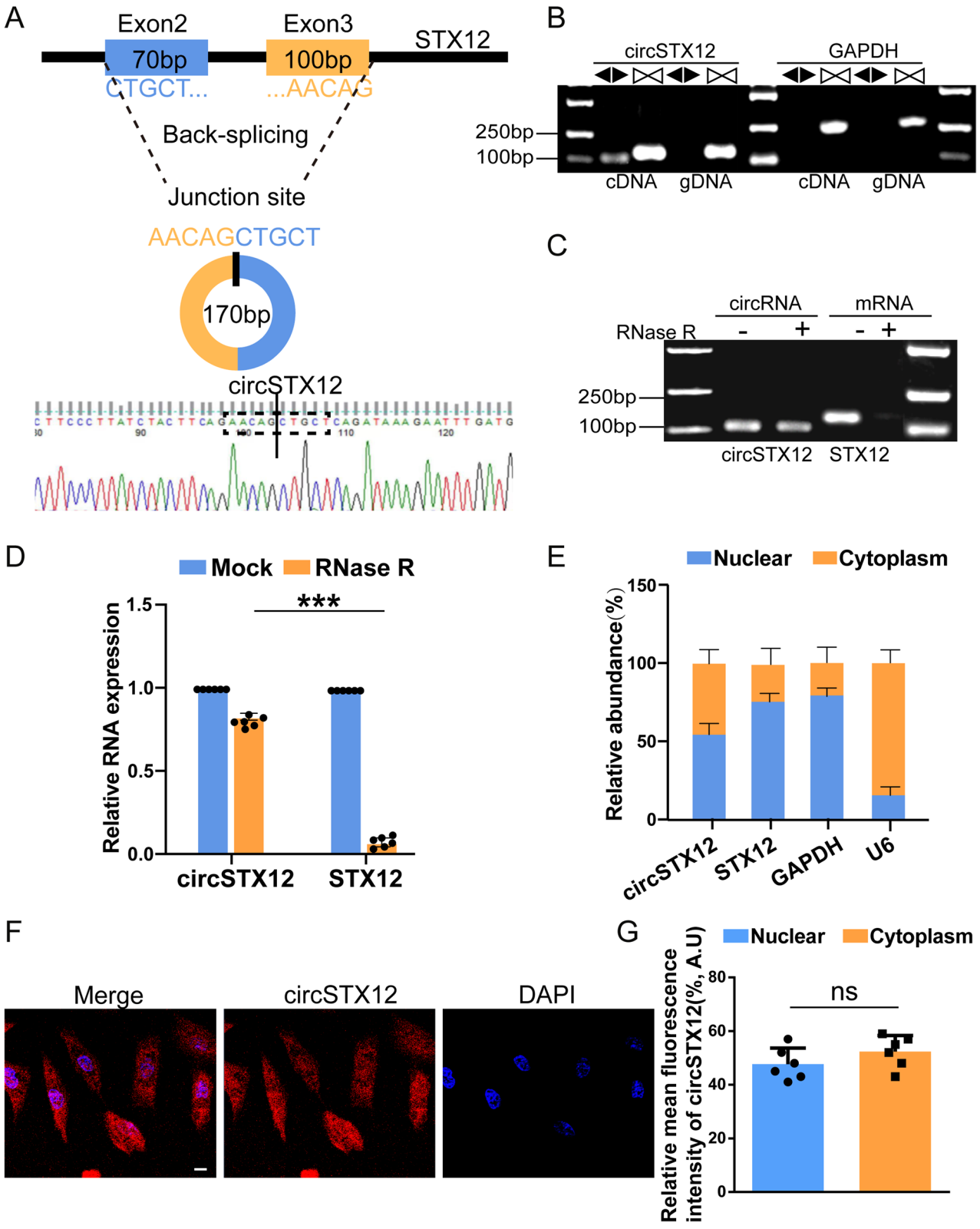
A
Exon2
Exon3
STX12
70bp
100bp
CTGCT...
...AACAG
Back-splicing
Junction site
AACAGCTGCT
170bp
circSTX12
B
circSTX12
GAPDH
250bp
100bp
cDNA
gDNA
cDNA
gDNA
C
circRNA
mRNA
RNase R
-
+
-
+
250bp
100bp
circSTX12
STX12
D
Mock
RNase R
***
Relative RNA expression
1.5
1.0
0.5
0.0
circSTX12
STX12
E
Nuclear
Cytoplasm
Relative abundance(%)
150
100
50
0
circSTX12
STX12
GAPDH
U6
F
Merge
circSTX12
DAPI
G
Nuclear
Cytoplasm
Relative mean fluorescence intensity of circSTX12(%, A.U)
ns
80
60
40
20
0

Fig. 1 The characteristics of circSTX12. Schematic of exons 2 and 3 of the STX12 mRNA, which is located on human chromosome 1 and gives rise to the 170-nucleotide-long circSTX12 and details of the sequence junction. **B**. The presence of circSTX12 in BMSCs was validated by RT-PCR. Divergent primers (◀▶) amplified circRNAs from cDNA but not from genomic DNA (gDNA). (▷◁) indicates convergent primers. **C**.The DNA electrophoresis results of RT-PCR of circSTX12 and STX12 mRNA in BMSCs treated with or without RNase R. **D.** Histogram showed that the degree of decrease in the expression of circSTX12 was significantly less than that of its parental gene after RNase R treatment. $n=6$ BMSCs samples. **E.** Nuclear and cytoplasmic RNA extraction and qPCR revealed that circSTX12 was uniformly distributed in the cytoplasm and nucleus. $n=3$ BMSCs samples. **F**. FISH was used to visualize the subcellular distribution of circSTX12. The nuclei were stained with DAPI. Scale bar =20 μm. **G**. The relative mean fluorescence intensity of circSTX12 in the FISH assay of panel F. $n=6$ biological replicates. The data are presented as the mean ± SEM..***$p<0.001$. ns: no significance

by qPCR, which revealed that circSTX12 was distributed in both the cytoplasm and the nucleus of BMSCs (Fig. 1E), which was further validated by fluorescence in situ hybridization (FISH) (Fig. 1F and G).

CircSTX12 expression in BMSCs increases with age

T-score evaluated after a dual energy X-ray absorptiometry (DXA) examination on the lumbar spine was taken as criterion to classify the populations into three groups: young control group (healthy donor, $n=11$, mean age = 22.5 ± 3.8 y), osteopenia group ($n=9$, mean age = 55.4 ± 2.9 y, mean T-score = -1.70 ± 0.50) and osteoporotic group ($n=10$, mean age = 76.0 ± 7.8 y, mean T-score = -2.59 ± 0.30). Bone tissue sections of different groups were made, and fluorescence in situ hybridization (FISH) for circSTX12 was performed (Fig. 2A). The bone tissue protein of different groups was extracted, and western blot for OCN was performed (Fig. 2B). The BMSCs were isolated as previously described [24, 25]. The expression level of circSTX12 in both bone tissues and BMSCs was greater in patients with osteopenia group and osteoporotic group than in that of young control group, as determined by FISH and qPCR (Fig. 2A and C). The increase in circSTX12 expression in BMSCs with age was also observed in human donors aged 20 to 80 years old (Fig. 2D). Moreover, circSTX12 levels in BMSCs of different ages were positively correlated with those of the cellular senescence marker p16 (Fig. 2D and E). This positive correlation was recapitulated in cultures of human BMSCs expanded in vitro for passage 3, 6 and 12 (P3, P6 and P12) (Fig. 2F and G). Moreover, the upregulation of circSTX12 was also verified in an H_2O_2-stimulated model of cell senescence (Fig. 2H). Collectively, these observations indicated that the upregulation of circSTX12 is concurrent with osteoporosis and is positively correlated with the progression of BMSCs senescence.

Moreover, we also detected simultaneously the expression levels of other circRNAs found in our sequencing that have a significant effect on osteogenic differentiation, like hsa_circ_0000348, hsa_circ_0001493 and hsa_circ 0070562 [23] and other circRNAs spliced fiom the same parent gene STX12, like has_circ_0005672 and hsa_circ_0112943, in BMSCs of osteoporosis, compared with that of HD, Results showed that there were no significant difference in the expression levels of these circRNAs in BMSCS of osteoporosis compared with that of HD (Supplementary Fig. 1A).

CircSTX12 inhibits osteogenesis and promotes adipogenesis in BMSCs

To investigate the role of circSTX12 in the regulation of BMSCs differentiation, we first analysed the level of circSTX12 expression during the osteogenic or adipogenic differentiation of human BMSCs. The results showed that the level of circSTX12 decreased markedly during osteogenic differentiation (Fig. 3A). In contrast, it was increased during adipogenic differentiation (Fig. 3B). Next, we overexpressed and knocked down circSTX12 in BMSCs via plasmids and ASOs respectively. The RT-qPCR results showed that the ASOs significantly decreased the expression of circSTX12 (Supplementary Fig. 1B and 1C), and the circSTX12 overexpression plasmids increased the expression of circSTX12 in BMSCs (Supplementary Fig. 1D). Neither overexpression nor knockdown affected the expression of STX12 mRNA (Supplementary Fig. 1C and 1D). Knockdown of circSTX12 enhanced alkaline phosphatase (ALP) staining and ALP activity, and circSTX12 overexpression counteracted these effects in BMSCs cultured in osteogenic medium for 7 days (Fig. 3C). Decreased expression of circSTX12 promoted the formation of calcium nodules, while circSTX12 overexpression counteracted these effects in BMSCs after 14 days of induction in osteogenic medium, as detected by alizarin red staining (ARS) (Fig. 3D). Consistent with these findings, circSTX12 knockdown induced OPN, OCN and RUNX2 expression highly at the mRNA and protein levels compared with the control and circSTX12 overexpression counteracted these effects (Fig. 3E and F). Taken together, these results indicated that circSTX12 negatively regulates osteogenesis. We next investigated the function of circSTX12 in the regulation of adipogenesis in BMSCs. In marked contrast to the osteogenic process, although control BMSCs began to undergo adipogenic differentiation after 14 days of culture under adipogenic conditions, weaker ORO staining and lower mRNA and protein levels of the adipogenic markers PPARG, FABP4 and CEBPA were observed upon circSTX12 knockdown compared with the NC, while rescue experiments with overexpression restored

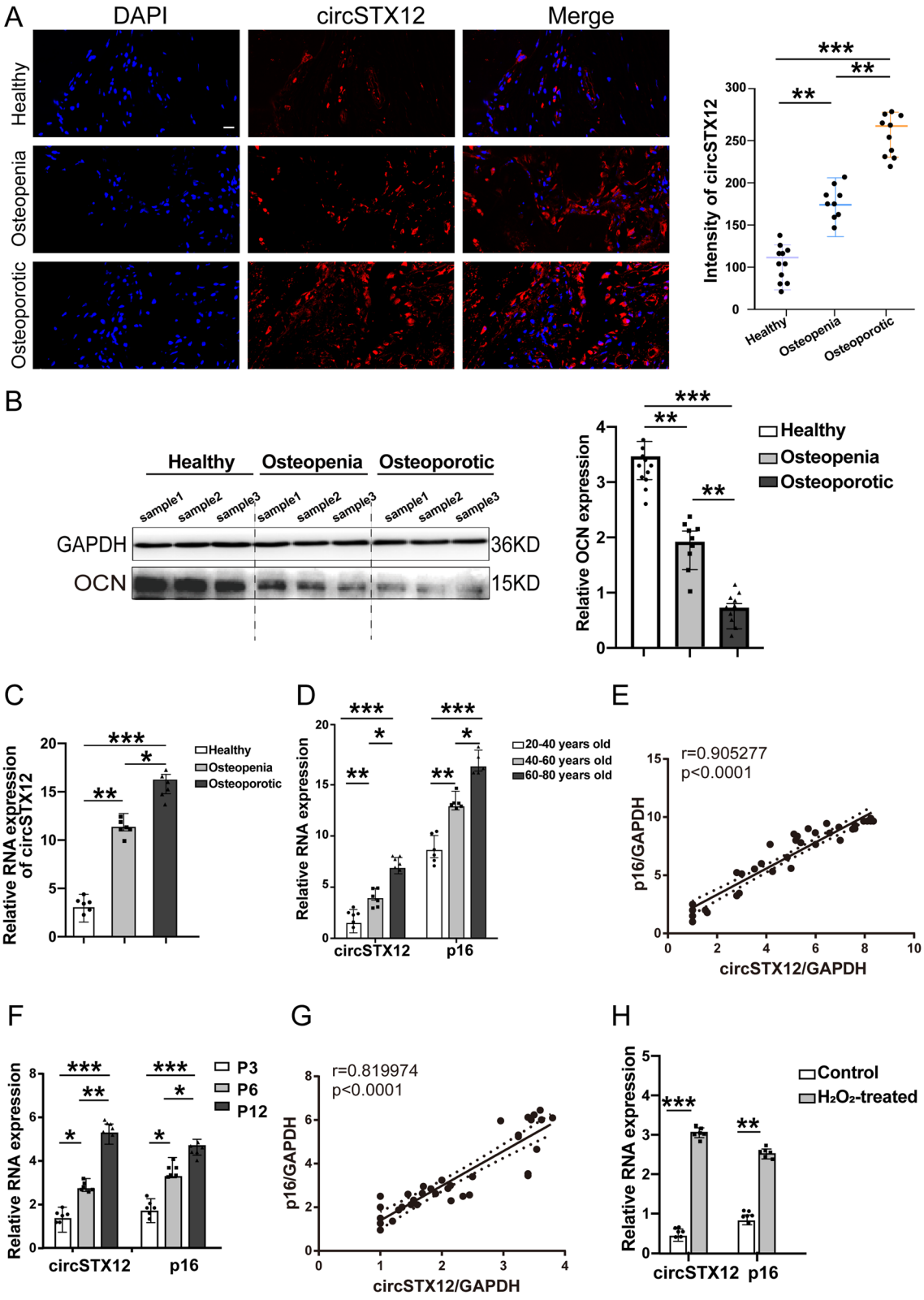
A
DAPI
circSTX12
Merge
Healthy
Osteopenia
Osteoporotic
Intensity of circSTX12
B
Healthy
Osteopenia
Osteoporotic
sample1
sample2
sample3
GAPDH
OCN
36KD
15KD
Relative OCN expression
C
Relative RNA expression of circSTX12
D
Relative RNA expression
20-40 years old
40-60 years old
60-80 years old
circSTX12
p16
E
r=0.905277
p<0.0001
p16/GAPDH
circSTX12/GAPDH
F
Relative RNA expression
P3
P6
P12
G
r=0.819974
p<0.0001
H
Control
H₂O₂-treated

Fig. 2 CircSTX12 expression in BMSCs increases with age. **A.** Bone tissue sections of different groups(young control group (healthy donor, $n=11$, mean age = 22.5 ± 3.8 y), osteopenia group ($n=9$, mean age = 55.4 ± 2.9 y, mean T-score = -1.70 ± 0.50) and osteoporotic group ($n=10$, mean age = 76.0 ± 7.8 y, mean T-score = -2.59 ± 0.30)) were made, and fluorescence in situ hybridization (FISH) for circSTX12 was performed. DAPI (blue) and circSTX12 (red). The intensity of circSTX12-positive cells was determined by ImageJ. Scale bar = 50 μm. **B**. Western blot and quantification of the OCN levels in bone tissue of healthy donor, osteopenia group and steoporotic group. (healthy donor $n=11$, osteopenia group $n=9$ and osteoporotic group $n=10$). **C**. RT-qPCR results of circSTX12 in BMSCs of healthy donor, osteopenia group and steoporotic group $n=6$ biological replicates. **D**. RT-qPCR results of circSTX12 and p16 accumulated gradually in BMSCs of donors with ageing from 20 to 80 years old. $n=6$ biological replicates. **E**. A Pearson correlation test revealed a strong positive relationship between circSTX12 and p16 expression in BMSCs of donors with ageing from 20 to 80 years old. **F**. RT-qPCR results indicated that the expression of circSTX12 and p16 were increased in vitro in BMSCs at passage 3, 6 and 12 (P3, P6 and P12). $n=6$ biological replicates. **G**. A Pearson correlation test revealed a positive relationship between circSTX12 and p16 expression in cultured BMSCs at P3, P6 and P12. **H**. RT-qPCR results showed that the expression of circSTX12 and p16 was up-regulated in H_2O_2-treated BMSCs. $n=6$ biological replicates. The data are presented as the mean ± SEM. $*p<0.05$, $**p<0.01$, $***p<0.001$

these effects(Fig. 3G, H and I). These results demonstrated the positive effects of circSTX12 on adipogenic differentiation. Taken all together, circSTX12 inhibits osteogenesis and promotes adipogenesis in BMSCs.

Hippo/YAP signaling mediates the regulatory effect of circSTX12 on BMSCs differentiation

We next sought to determine the molecular mechanism by which circSTX12 controls the cell fate of BMSCs. BMP/Smad, Hippo/YAP, Wnt/β-catenin and Hedgehog/Gli etc. are canonical pathways that regulate BMSCs adipo-osteogenic balance [26–30]. We observed that the level of p-YAP was obviously reduced during BMSCs osteogenic differentiation in circSTX12-knockdown BMSCs compared with controls, and in line with these findings, the level of YAP was obviously increased in circSTX12-knockdown BMSCs during osteogenic differentiation; while circSTX12 overexpression counteracted these effects (Fig. 4A). Additionally, knockdown of circSTX12 promoted the nuclear localization of YAP (Fig. 4B). However, other signaling pathways, such as BMP/Smad, Wnt/β-catenin and Hedgehog/Gli pathways, were almost unchanged among the circSTX12 knockdown, circSTX12 overexpression and control groups (Fig. 4A). We further applied a YAP inhibitor to verify the role of YAP in circSTX12-mediated regulation of BMSCs differentiation. BMSCs were treated with 1.25, 2.5 or 5 nM of YAP inhibitor. At 2.5 nM, the YAP inhibitor obviously inhibited BMSCs osteogenesis (Supplementary Fig. 2A). Therefore, we chose 2.5 nM of the inhibitor for subsequent experiments. As expected, in the circSTX12-knockdown BMSCs, 2.5 nM YAP inhibited the enhanced formation of calcium nodules after 14 days of induction in osteogenic medium and counteracted the decreased ORO staining after 14 days of adipogenic induction (Fig. 4C). These results suggest that circSTX12 controls BMSCs differentiation primarily through the regulation of YAP. The Hippo signaling pathway has conserved functions in regulating cell proliferation and differentiation by controlling the phosphorylation and cytosolic-nuclear localization of YAP. MST1/2 and LATS1/2 are two upstream kinases that contribute to YAP phosphorylation [31]. To test whether MST1/2 and LATS1/2 are involved in the circSTX12-mediated regulation of YAP and consequent BMSCs differentiation, we conducted immunoblotting to test the expression and activity of MST1/2 and LATS1/2 in circSTX12-deficient and circSTX12-overexpressing BMSCs, respectively. Similar to the p-YAP level, the expression of MST1, and the activity of MST1/2 and LATS1 were obviously decreased in the circSTX12-deficient BMSCs while circSTX12 overexpression counteracted these effects (Fig. 4A). We then designed MST1 overexpression and knockdown vectors, and verified the knockdown and overexpression efficiency of MST1 (Supplementary Fig. 3A and 3B). Results demonstrated that overexpression of MST1 in circSTX12-deficient BMSCs rescued the levels of p-YAP, decreased the level of YAP and ARS assay, and increased the ORO assay (Fig. 4D and E), compared with that in the circSTX12-deficient group. Whereas knockdown of MST1 in circSTX12-overexpressed BMSCs decreased the levels of p-YAP, rescued the level of YAP and ARS assay, and counteracted the ORO assay (Fig. 4F and G), compared with that in the circSTX12-overexpressed group. These results suggest that the level of MST1 is involved in circSTX12-mediated regulation of YAP and BMSCs osteo-adipogenic differentiation. Moreover, MST1 mRNA expression was not altered in circSTX12-deficient BMSCs (Fig. 5A) and the decrease in MST1 protein expression induced by circSTX12 knockdown could be attenuated by application of the proteasome inhibitor MG132 (Fig. 5B). Collectively, these results suggested that the expression of MST1, mediated by protein degradation, is involved in the regulation in YAP levels and effects on BMSCs differentiation mediated by circSTX12.

CircSTX12 competitively binds to CBL to decrease MST1 ubiquitination

To further explore the mechanism by which circSTX12 regulates the balance between osteogenic and adipogenic differentiation in BMSCs, we performed RNA pulldown assays of circSTX12 using biotinylated probes targeting the circSTX12 back-spliced sequence and subjected the

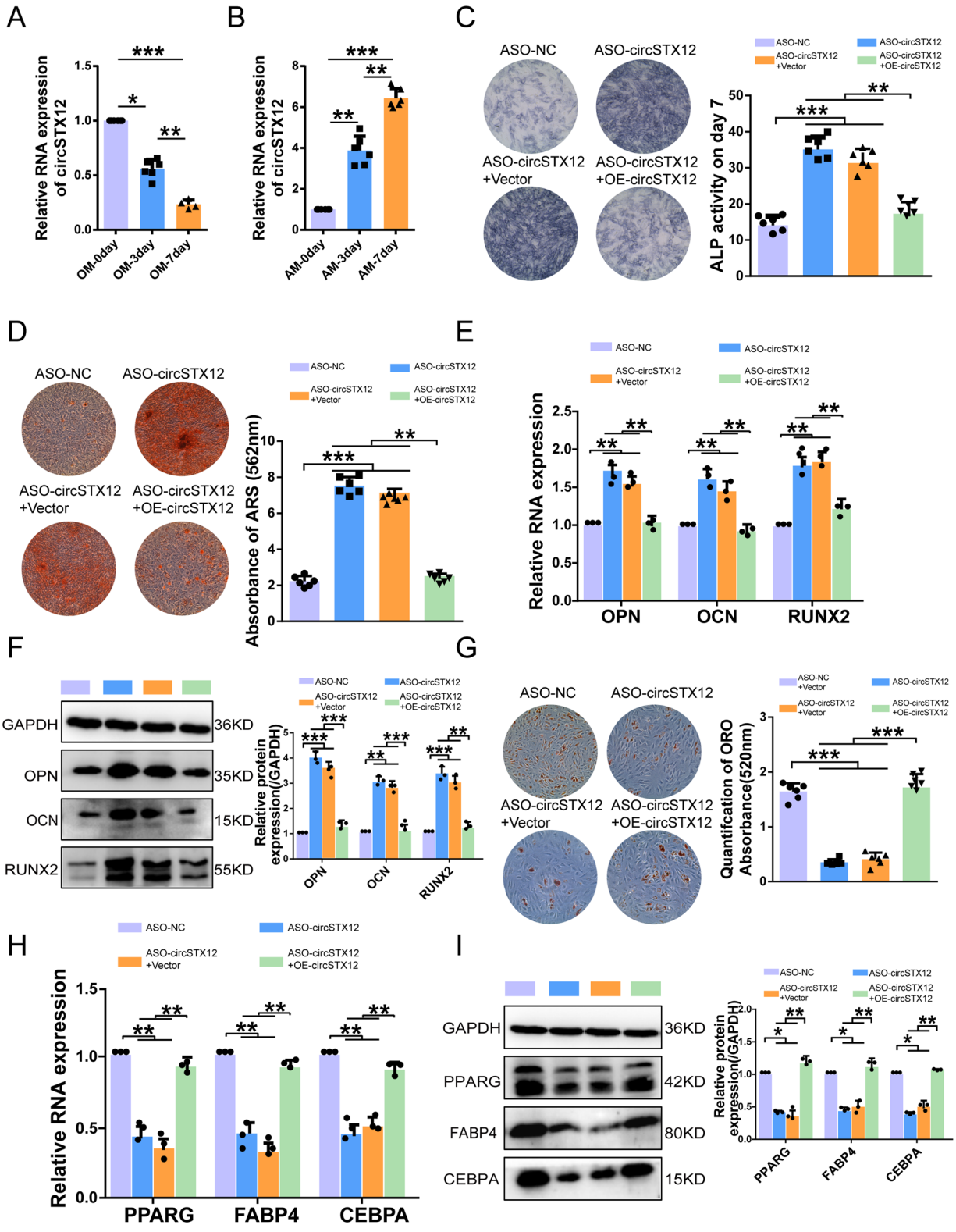
A
Relative RNA expression of circSTX12
OM-0day
OM-3day
OM-7day
B
Relative RNA expression of circSTX12
AM-0day
AM-3day
AM-7day
C
ASO-NC
ASO-circSTX12
ASO-circSTX12 +Vector
ASO-circSTX12 +OE-circSTX12
ALP activity on day 7
D
Absorbance of ARS (562nm)
E
Relative RNA expression
OPN
OCN
RUNX2
F
GAPDH
OPN
OCN
RUNX2
36KD
35KD
15KD
55KD
Relative protein expression/(GAPDH)
G
Quantifcation of ORO Absorbance(520nm)
H
Relative RNA expression
PPARG
FABP4
CEBPA
I
GAPDH
PPARG
FABP4
CEBPA
36KD
42KD
80KD
15KD
Relative protein expression/(GAPDH)

Fig. 3 CircSTX12 inhibits osteogenesis and promotes adipogenesis in BMSCs. **A.** RT-qPCR results indicated the circSTX12 expression on day 0, 3, 7 in ostegenic medium (OM). **B**. RT-qPCR results indicated the circSTX12 expression on day 0, 3, 7 in adipogenic medium (AM). **C.** ALP staining and ALP activity in BMSCs with circSTX12 knockdown or knockdown rescue experiment. **D**. ARS staining and quantification of BMSCs with circSTX12 knockdown or knockdown rescue experiment. **E**. RT-qPCR results of the expression of osteogenesis-related mRNAs in circSTX12 knockdown or knockdown rescue experiment BMSCs or the control. **F.** Western blot and quantification of the levels of OPN, OCN, and RUNX2 in BMSCs with circSTX12 knockdown or knockdown rescue experiment. **G.** ORO staining and quantification of BMSCs with circSTX12 knockdown or knockdown rescue experiment. **H**. RT-qPCR results of the expression of PPARG, FABP4 and CEBPA in circSTX12 knockdown or knockdown rescue experiment. **I.** Western blot and quantification of the Protein levels of PPARG, FABP4 and CEBPA in circSTX12 knockdown or knockdown rescue experiment. $n=3$ biological replicates. The data are presented as the mean ± SEM; $n=6$ biological replicates in panel A-D and panel G. $n=3$ biological replicates in panel E, F, H and I. $^{*}p<0.05$, $^{**}p<0.01$, $^{***}p<0.001$

precipitates to mass spectrometry analysis. Several binding proteins were identified, the most abundant of which included CBL (Fig. 5C). We then confirmed the interaction between circSTX12 and CBL using RNA pull-down followed by Western blot (Fig. 5D) and RNA immunoprecipitation (RIP) (Fig. 5E). CBL was originally identified as a cytosolic RING finger domain ubiquitin E3 ligase that ubiquitinates various receptor tyrosine kinases (RTKs) and RTK substrates, and regulates cell proliferation, survival, and motility [32]. In light of our findings that MST1 degradation is involved in circSTX12 function and previous reports that MST1 is an RTK substrate [33], we wondered whether CBL could ubiquitinate and degrade MST1. Coimmunoprecipitation confirmed that CBL and MST1 can interact with each other (Fig. 5F and G). We designed the siRNAs of CBL and verified their efficiency(Supplementary Fig. 4A), and we found that CBL knockdown increased the expression of MST1 (Fig. 5H). Then we used MG132 to block the ubiquitin-proteasome-dependent degradation of MST1, and used primary antibody of MST1 to precipitate the MST1 and the interacting proteins. Indeed, silencing CBL led to a significant decrease in MST1 ubiquitylation in BMSCs after osteogenic induction for 7 days (Fig. 5I and J). Meanwhile, the altered expression of circSTX12 affected the interaction between CBL and MST1. CircSTX12 knockdown did not affect CBL expression (Supplementary Fig. 2B), but significantly enhanced the binding of CBL to MST1 (Fig. 5I and K) and enhanced the ubiquitination of MST1 (Fig. 5I and J). Moreover, silencing of CBL increased MST1 protein level by decreasing the ubiquitination of MST1, which abrogated the pro-ubiquitination effect on MST1 after circSTX12 knockdown (Fig. 5I and J). Finally, we further confirmed that CBL mediated the impact of circSTX12 on BMSCs differentiation in vitro. We performed rescue experiments and found that silencing CBL could reverse the pro-osteogenesis and anti-adipogenesis effect of circSTX12 silencing (Fig. 5L and M). Collectively, these data demonstrate that circSTX12 competitively binds to CBL and interferes with MST1 degradation, ultimately accounting for BMSCs adipo-osteogenic differentiation.

CircSTX12 inhibits BMSCs proliferation

To explore the role of circSTX12 in BMSCs proliferation, CCK-8 assays, cloning assays, cell cycle assays and EdU staining were performed on BMSCs after modulation of circSTX12 expression. The results of the CCK-8 assay showed that circSTX12 knockdown significantly increased the cell viability of BMSCs, while circSTX12 overexpression counteracted these effects (Fig. 6A). BMSCs are colony-forming cells in culture and are also sometimes called colony-forming unit-fibroblasts (CFU-Fs) [34]. We found that knocking down circSTX12 increased the clonal expansion ability of these cells, while circSTX12 overexpression counteracted these effects (Fig. 6B and C). In addition, flow cytometry showed that circSTX12 knockdown increased the S- and G2/M-phase ratios of the cell cycle in BMSCs, while circSTX12 overexpression counteracted these effects (Fig. 6D and E). Consistent with the above results, EdU staining indicated that the percentage of EdU-positive cells was greater in the circSTX12 knockdown group than in the control group, while the circSTX12 overexpression group counterbalanced these effects (Fig. 6F and G). Taken together, these data demonstrate that circSTX12 negatively regulates BMSCs proliferation in vitro.

CircSTX12 binds to and sequesters LMO7 in the cytoplasm

To determine how circSTX12 inhibits BMSCs proliferation, we firstly detected the change of MST1/YAP signaling pathway in BMSCs with circSTX12 knockdown or overexpression for 48 h and 72 h in basic medium, as MST1/YAP signaling pathway plays important role in cell proliferation besides differentiation. Results showed that neither the level of MST1 or YAP was changed in BMSCs with circSTX12 knockdown, or overexpression, compared with the NC group, after cultured in the basic medium for 48 h and 72 h, in which time point the pro-proliferative effect of circSTX12 on BMSCs had appeared. (Supplementary Fig. 5A and Fig. 6A). We then further screened the mass spectrometry results from the RNA pull-down assay of circSTX12 using biotinylated probes targeting the circSTX12 back-spliced sequence. LMO7 was found among the most abundant protein candidates (Fig. 7A). RNA pull-down assay combined with Western blot confirmed that LMO7

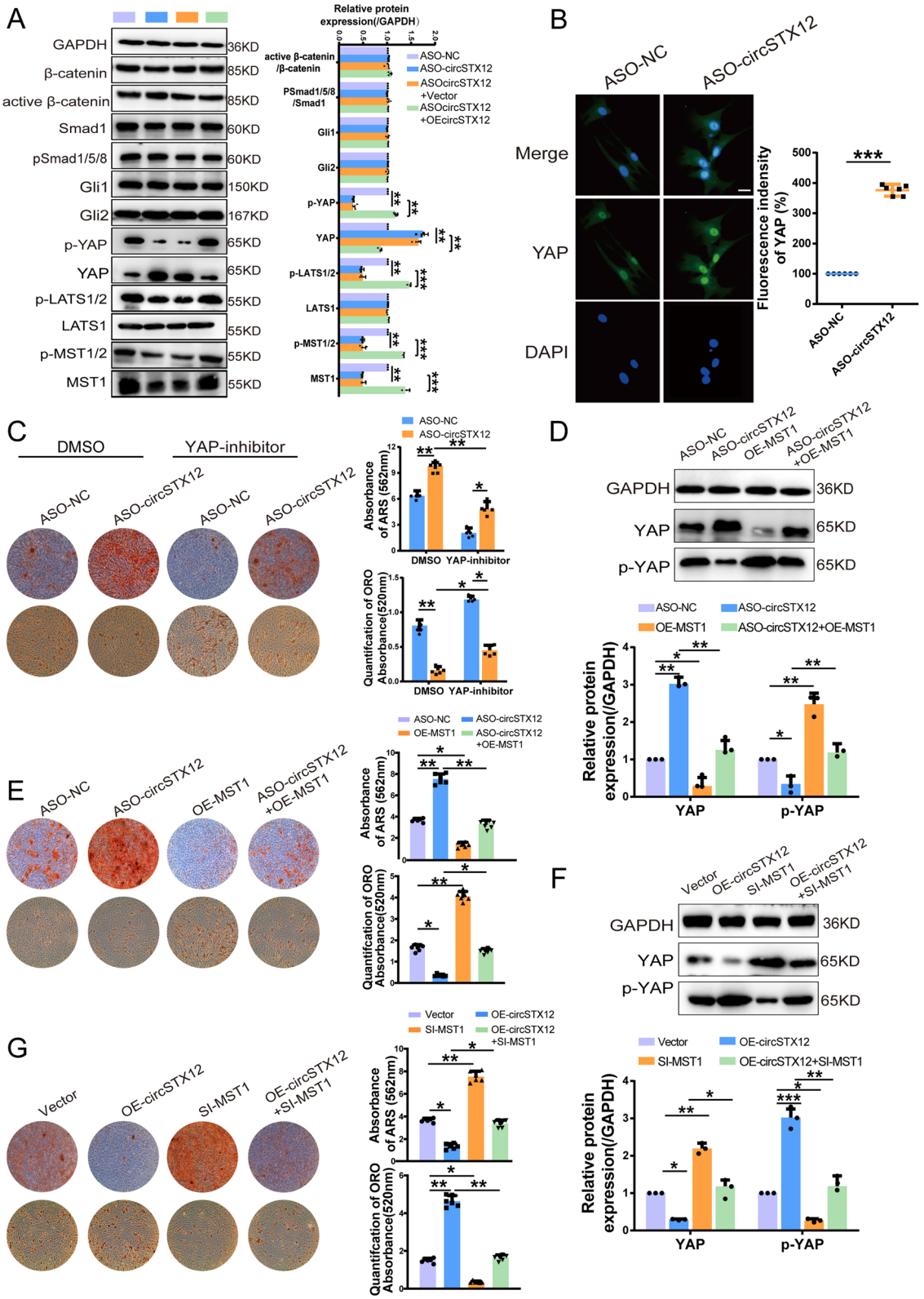
A
GAPDH
β-catenin
active β-catenin
Smad1
pSmad1/5/8
Gli1
Gli2
p-YAP
YAP
p-LATS1/2
LATS1
p-MST1/2
MST1
36KD
85KD
85KD
60KD
60KD
150KD
167KD
65KD
65KD
55KD
55KD
55KD
55KD
Relative protein expression(/GAPDH)
active β-catenin /β-catenin
PSmad1/5/8 /Smad1
ASO-NC
ASO-circSTX12
ASOcircSTX12 +Vector
ASOcircSTX12 +OEcircSTX12
B
ASO-NC
ASO-circSTX12
Merge
YAP
DAPI
Fluorescence indensity of YAP (%)
C
DMSO
YAP-inhibitor
Absorbance of ARS (562nm)
Quantifcation of ORO Absorbance(520nm)
D
OE-MST1
ASO-circSTX12+OE-MST1
Relative protein expression(/GAPDH)
E
OE-circSTX12
SI-MST1
OE-circSTX12 +SI-MST1
F
G

Fig. 4 Hippo/YAP signaling mediates circSTX12-related regulation of BMSCs differentiation. **A.** Western blot analysis of the expression of proteins involved in adipo-osteogenic pathways in circSTX12 knockdown or knockdown rescue experiment in BMSCs after 7 days' induction in osteogenic medium. $n=3$ biological replicates. **B**. Immunofluorescence analyses of YAP in BMSCs with circSTX12 knockdown or the control. $n=6$ biological replicates. YAP (green) and DAPI (blue). Scale bar = 200 μm. **C**. ARS and ORO staining and quantification assays results on day 14 in circSTX12 knockdown and the control BMSCs after incubated in adipogenic and osteogenic medium containing 2.5 nM YAP inhibitor or not. $n=6$ biological replicates. **D**. Left panel showed the Western blot results of YAP and p-YAP protein levels in BMSCs transfected with ASO-NC, ASO-circSTX12, OE-MST1, or ASO-circSTX12 + OE-MST1. Right panel showed the histogram result in left panel. $n=3$ biological replicates. **E**. ARS and ORO staining and quantification assays results on day 14 in BMSCs transfected with ASO-NC, ASO-circSTX12, OE-MST1, or ASO-circSTX12 + OE-MST1. $n=6$ biological replicates. **(F)** Left panel showed the Western blot results of YAP and p-YAP protein levels in BMSCs transfected with Vector, OE-circSTX12, SI-MST1, or OE-circSTX12 + SI-MST1. Right panel showed the histogram result in left panel. $n=3$ biological replicates. **(G)** ARS and ORO staining and quantification assays results on day 14 in BMSCs transfected with Vector, OE-circSTX12, SI-MST1, or OE-circSTX12 + SI-MST1. Right panel showed the histogram result in left panel. $n=6$ biological replicates. All the data are presented as the mean ± SEM. $^{*}p<0.05$, $^{**}p<0.01$, $^{***}p<0.001$

bound to circSTX12 (Fig. 7B). Moreover, an RIP assay also indicated that endogenous LMO7 interacted with circSTX12 in BMSCs (Fig. 7C), further verifying the specificity of circSTX12 and LMO7 binding. Previous reports have shown that LMO7 localizes to the nucleus in myoblasts and plays a pivotal role in myogenesis [35]. LMO7 deficiency suppressed cell proliferation and colony formation in cancer cells [36]. However, whether LMO7 regulates the proliferation of BMSCs has not yet been reported. In our immunofluorescence experiment, we found that LMO7 was highly expressed in BMSCs and was more abundant in the nuclei of early-passage BMSCs than in the nuclei of later-passage BMSCs (Supplementary Fig. 6A). Then we designed the siRNAs of LMO7 and verified their efficiency(Supplementary Fig. 4B), Consistent with these findings, LMO7 knockdown inhibited BMSCs proliferation, as indicated by assays of clonal expansion ability (Fig. 7D and E), cell cycle distribution (Fig. 7F and G) and EdU staining (Fig. 7H and I). Moreover, LMO7 knockdown reversed the pro-proliferative effect of circSTX12 knockdown (Fig. 7D and I). Overall, these findings indicate that LMO7 binds to circSTX12 and mediates the role of circSTX12 in regulating BMSCs proliferation. LMO7 was reported to be a transcription activator that regulates the expression of myoblast proliferation genes and myoblast differentiation [37]. Endogenous LMO7 is a nucleocytoplasmic shuttling protein [38]. Both immunofluorescence staining (Fig. 6J and K) and nucleocytoplasmic cell isolation (Fig. 6L) demonstrated that circSTX12 defects led to increased transport of the LMO7 protein into the nucleus but decreased level of this protein in the cytoplasm, while ectopic expression of circSTX12 promoted the cytoplasmic distribution of LMO7. These results further confirmed that circSTX12 could bind and sequester LMO7 in the cytoplasm to inhibit BMSCs proliferation.

CircSTX12/LMO7 affects the transcription of CCNA2, CCNH and CCND1

Next, we used CUT&Tag-seq to explore the molecular mechanism by which LMO7 promotes BMSCs proliferation after circSTX12 knockdown. Heatmaps revealed general CUT&Tag-seq signals for LMO7 occupancy in chromatin (Supplementary Fig. 7A) and in gene bodies (Supplementary Fig. 7B) after circSTX12 knockdown. The differential peaks between the circSTX12 knockdown group and the control group were mostly distributed in promoter, intron and distal intergenic regions (Fig. 8A). KEGG biological process analysis revealed that the LMO7-occupied genes in the circSTX12 knockdown group were enriched in terms related to the cell cycle and p53 signaling pathway, which regulate the cell proliferation process [39] (Fig. 8B and Supplementary Table 3). The differentially expressed genes (DEGs) associated with these two terms included CCNA2, CCNH, CCND1, CCNG2, and others (Fig. 8C). Specifically, the occupancy of LMO7 on the promoter region of CCNA2 and CCNH (Fig. 8D) and in the distal intergenic region of CCND1 (Fig. 8E) was greater in the circSTX12 knockdown group than in the NC group, as indicated by the red frame. Moreover, the RNA expression of CCNA2, CCNH and CCND1 was up-regulated after circSTX12 knockdown but down-regulated after circSTX12 overexpression, and LMO7 knockdown reversed the up-regulated effect of circSTX12 silencing (Fig. 8F). While among other DEGs in Fig. 8C, we did not see obvious differences in the occupancy of LMO7 CUT&Tag-seq or in the RNA levels detects in BMSCs after circSTX12 knockdown or overexpression (data not shown). Taken together, these data suggest that LMO7 modulates the transcription of CCNA2, CCNH and CCND1 to mediate circSTX12-induced BMSCs proliferation.

Targeting circStx12 inhibits OP development in an aged mice model

Given that circSTX12 is increased in senile osteoporosis, and that circSTX12 knockdown can promote osteogenic differentiation, inhibit adipogenic differentiation and increase proliferation of BMSCs in vitro, we further explored the effect of circStx12 knockdown on bone regeneration via circStx12-specific ASOs for use in vivo in aged mice. Exons 2 and 3 of STX12 were found to be highly conserved between humans and mice, with a similarity of

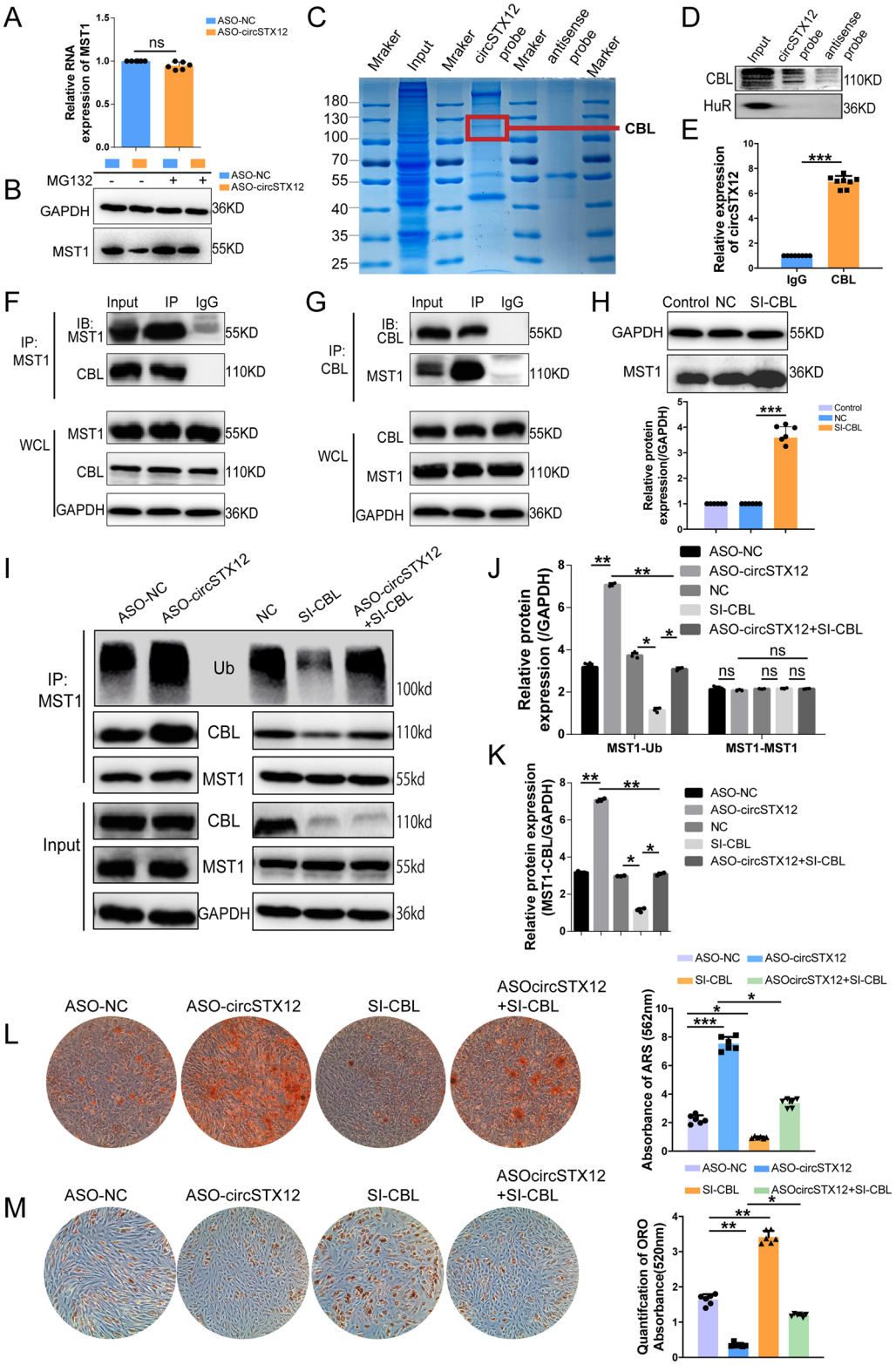
A
Relative RNA expression of MST1
ns
ASO-NC
ASO-circSTX12
B
MG132
GAPDH
MST1
36KD
55KD
C
Mraker
Input
circSTX12 probe
antisense probe
Marker
CBL
D
CBL
HuR
110KD
36KE
E
Relative expression of circSTX12
IgG
CBL
F
Input
IP
IgG
IP: MST1
IB: MST1
CBL
WCL
G
IP: CBL
IB: CBL
H
Control
NC
SI-CBL
Relative protein expression(/GAPDH)
I
ASO-NC
ASO-circSTX12
NC
SI-CBL
ASO-circSTX12 +SI-CBL
Ub
100kd
110kd
55kd
36kd
Input
J
Relative protein expression (/GAPDH)
MST1-Ub
MST1-MST1
K
Relative protein expression (MST1-CBL/GAPDH)
L
ASOcircSTX12 +SI-CBL
Absorbance of ARS (562nm)
M
Quantification of ORO Absorbance(520nm)

Fig. 5 CircSTX12 competitively binds to CBL to decrease MST1 ubiquitination. **A**. RT-qPCR results indicated the MST1 mRNA expression in BMSCs with circSTX12 knockdown. $n=6$ biological replicates. **B**. Western blot results of MST1 in BMSCs treated with or without MG132 after circSTX12 knockdown. $n=6$ biological replicates. **(C)** Coomassie brilliant blue staining followed by mass spectrometry was used to identify the circSTX12-protein complex pulled down by the circSTX12 probe in protein extracts from BMSCs. The red frame indicates CBL. **(D)** CBL and HuR detected after pulling down with a circSTX12 probe or antisense probe. CBL bound to circSTX12, while HuR did not. $n=6$ independent experiments. **(E)** RT-qPCR analysis of circSTX12 after RIP to evaluate the interaction between CBL and circSTX12 in BMSCs. $n=8$ biological replicates. **F** and **G**. The interaction between CBL and MST1 in BMSCs was confirmed by immunoprecipitation followed by Western blot. WCL: whole cell lysate. **H.** Western blot results of the levels of MST1 in BMSCs with CBL knockdown. $n=6$ biological replicates. **I**. Cell lysates of BMSCs transfected with ASO-NC, ASO-circSTX12, SI-CBL or ASO-circSTX12 + SI-CBL with MG132 for 6 h (20 μM) before harvest were immunoprecipitated with an antibody against MST1 and analysed by immunoblotting with an ubiquitin (Ub)-specific antibody, an anti-MST1 antibody, or an anti-CBL antibody. **J.** Histogram result of the level of Ub and MST1 in the immunoprecipitates of MST1 with MG132 in panel I. $n=3$ biological replicates. **K**. Histogram result of the level of CBL in the immunoprecipitates of MST1 with MG132 in panel I. $n=3$ biological replicates. **L**. ARS staining and quantification of BMSCs transfected with NC or ASO-circSTX12 and CBL knockdown (SI-CBL) or not. $n=6$ independent experiments. **M.** ORO staining and quantification of BMSCs transfected with NC or ASO-circSTX12 and CBL knockdown (SI-CBL) or not. $n=6$ independent experiments. All the data are presented as the mean ± SEM. $^{*}p<0.05$, $^{**}p<0.01$, $^{***}p<0.001$

92% (Supplementary Fig. 8A). Then, we verified the backsplicing junction sequence of circStx12 by Sanger sequence analysis, which provided powerful evidence of the conservation of circStx12 in mice (Supplementary Fig. 8B). Then we designed the chemically modified ASOs for circStx12 used in vivo (Supplementary Fig. 8C). First, the effect of circStx12-specific ASOs on mice BMSCs was analysed in vitro, and the results demonstrated its ability to knockdown circStx12 expression and promote osteogenesis (Supplementary Fig. 8D and 8E). Next, we conducted preliminary experiments to test the effective dose and toxicity of tail-intravenous injection of circStx12 ASOs in mice. Results demonstrated that tail-intravenous injection of 10 nM of ASOs caused 60–70% down-regulation of circStx12 in femurs even after 2 weeks without toxicity in vivo (Supplementary Fig. 8F. Refer to the Materials and Methods for details). Then the dose of 10 nM of ASOs was chosen for the subsequent expanded sample size experiment. Physiologically aged mice (24 months old) were injected with control ASOs or circStx12 ASOs, and the 6 months young mice with saline and 24 months old mice with saline as the controls. Total of five injections were administered as once a week for two weeks and once two weeks for four weeks. Eight weeks after the first injection, the mice were sacrificed and the bone tissues and primary organs were collected (Fig. 9A). No significant changes in body or tissue weight were seen in the aged mice injected with circStx12 ASOs compared to those injected with the saline or control ASOs (Supplementary Fig. 8G). Additionally, circStx12 was expressed at greater levels in the bone tissue of the aged mice than in that of the control young mice, while 10 nM of circStx12 ASOs treatment significantly decreased the level of circStx12 (Fig. 9B). Next, we performed micro-CT and bone histomorphometric analysis to test the effect of circStx12 knockdown on bone regeneration. Micro-CT results showed that circStx12 ASOs treatment significantly prevented bone loss in aged mice. Static bone histomorphometric parameters including bone volume/total volume (BV/TV), and trabecular thickness (Tb.Th) and number (Tb.N) were significantly decreased, and the trabecular space (Th.Sp) was increased in aged mice compared with the young mice. However, circStx12 ASOs treatment withstood the changes in these parameters (Fig. 9C). H&E and Ocn immunohistochemical staining revealed that the trabecular bone area were significantly reduced and the adipocytes were increased in aged mice, but these effects were also partially rescued by circStx12 ASOs injection (Fig. 9D). Toluidine blue staining was used to quantify the number of osteoblasts and revealed that the number of osteoblasts was significantly reduced in aged mice(Fig. 9E and G). Immunohistochemistry staining of Perilipin-1 were performed to quantify the number of bone marrow adipocytes (Fig. 9F and H), which revealed that the adipocytes was increased in aged mice. But these effects were partially rescued by circStx12 ASOs injection(Fig. 9H). Dynamic histomorphometric studies by double calcein green injection showed that administration of circStx12 ASOs attenuated the suppression of bone formation in aged mice. We observed significant decreases in the mineralized surface/bone surface area (MS/BS), mineral accumulation rate (MAR), and bone formation rate per bone surface (BFR/BS) in aged mice, but these decreases were prevented by circStx12 ASOs treatment (Fig. 9E). Next, we performed tartrate-resistant acid phosphatase (TRAP) staining to investigate the properties of osteoclast in supplementary figure and the results showed that there was no significant difference in osteoclasts in mice femurs of the OP and OP + circStx12 ASOs groups (Supplementary Fig. 9) Taken together, the above results demonstrated that targeted circStx12 could promote bone formation to protect against osteoporosis in aged mice.

Discussion

Skeletal aging is a complex process, characterized by a decrease in bone formation, an increase in marrow fat, and stem cell exhaustion [40]. In this study, we uncover that circSTX12 is a critical epigenetic factor that controls

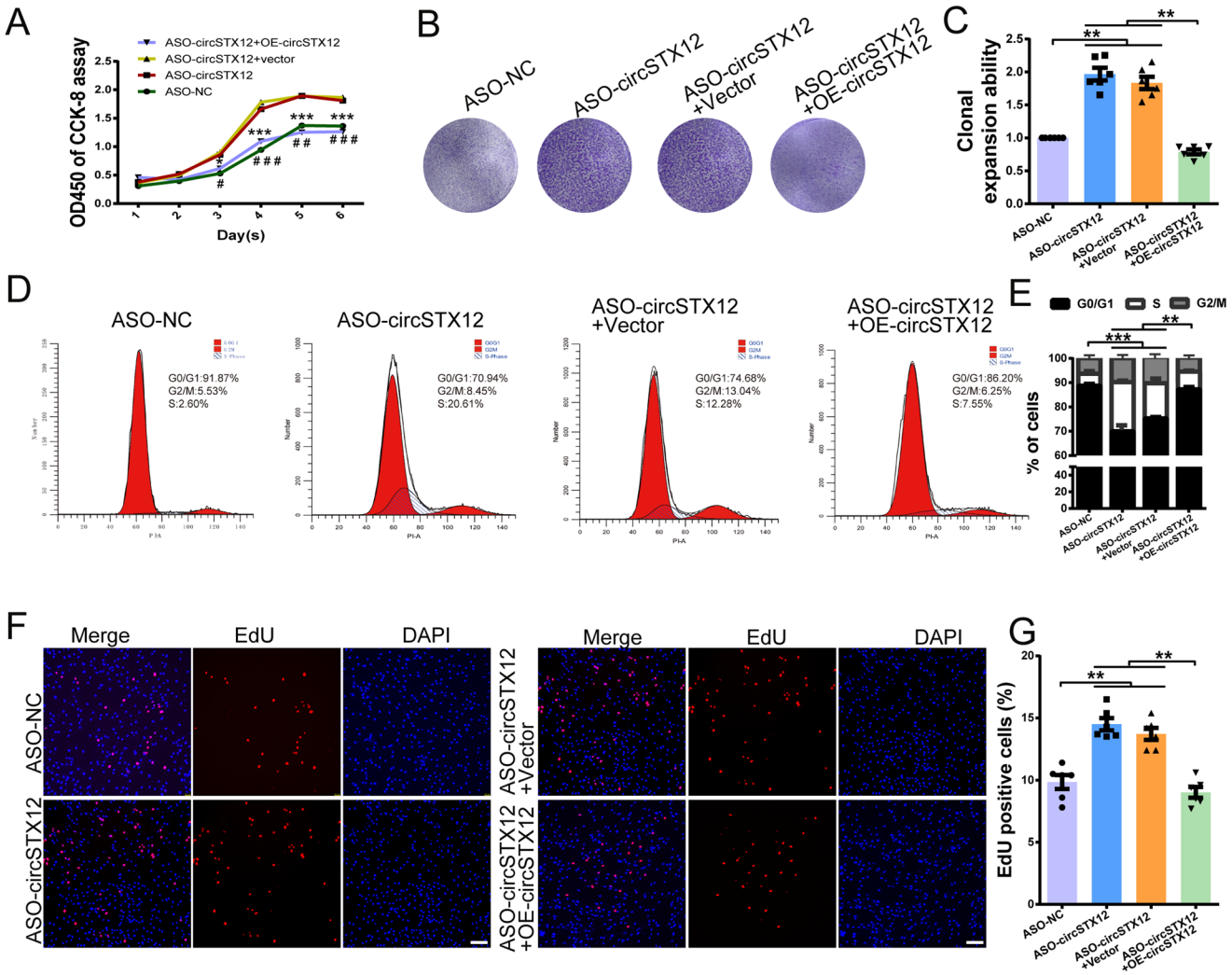

Fig. 6 CircSTX12 inhibits BMSCs proliferation. **A.** CCK-8 assay results for BMSCs with circSTX12 silencing or knockdown rescue experiment. and control BMSCs at day 0, 1, 2, 3, 4 and 5. "*" indicates ASO-NC vs. ASO-circSTX12 and ASO-circSTX12+Vector. "#" indicates ASO-circSTX12+OE-circSTX12 vs. ASO-circSTX12 and ASO-circSTX12+Vector. $n=6$ biological replicates. **B.** Clonal expansion of BMSCs in the circSTX12-silenced, knockdown rescue experiment and control groups. **C.** Histogram showing the analysis of the clonal expansion of BMSCs in which circSTX12 was silenced or knockdown rescue experiment and in the control groups shown in panel B. $n=6$ biological replicates. **D.** Flow cytometry analysis of the cell cycle distribution of BMSCs transfected with ASO-NC, ASO-circSTX12, ASO-circSTX12+vector, or ASO-circSTX12+OE-circSTX12 for 48 h. **E.** Histogram of the percentages of cells in the G0/G1, S, and G2/M phases of the cell cycle in panel D. The percentage of cells in different phases of cell cycle was analysed by FlowJo. $n=6$ biological replicates. **(F)** The results from the EdU staining of BMSCs transfected with ASO-NC, ASO-circSTX12, ASO-circSTX12+vector, or ASO-circSTX12+OE-circSTX12 for 48 h. Scale bar = 100 μm. **(G)** Histogram of the percentages of EdU-positive BMSCs with circSTX12 silencing or overexpression and control BMSCs in panel F. $n=6$ biological replicates. All the data are presented as the mean±SEM.* or # $p<0.05$, ** or ## $p<0.01$, ***or ### $p<0.001$

skeletal aging and osteoporosis. We found for the first time that circSTX12 is upregulated in bone tissue of senile osteoporosis and in the senescent BMSCs, and confirmed that circSTX12 negatively regulates the osteogenic differentiation and positively regulates adipogenic differentiation of BMSCs. Moreover, circSTX12 inhibits BMSCs proliferation. Our results suggest that circSTX12 might be a pivotal factor for controlling skeletal aging and osteoporosis.

CircRNAs have been shown to be epigenetic regulators with significant involvement in the control of gene expression, affecting multiple biological processes, including bone metabolism [41]. Recent years, increasing evidence supports the regulatory role of circRNAs in modulating the progress of osteoporosis [15, 42]. Due to the extensive data generated by high-throughput sequencing methods, the identification of osteoporosis-specific signatures associated with circRNAs became feasible. Until now thousands of circular transcripts involved in osteoporosis are listed and annotated. The studies of circRNA profilings in peripheral blood mononuclear cells (PBMCs) [43, 44], BMSCs [45,

46], exosomes derived from BMSCs [47] of patients with osteoporosis were published in very recent years. Several studies list various circRNAs, target molecules, pathways, and mechanisms that influence osteoporosis via promoting or inhibiting osteoblast or osteoclast differentiation and proliferation, depending on their target molecules and pathways. Like circRNA circAFF4 promotes osteoblast cells proliferation and inhibits apoptosis via the miR-7223-5p/PIK3R1 axis [48], circRNA_0016624 sponges miR-98 to regulate BMP2 expression [49], circRNA_28313 modulates CSF1 via miR-195a to affect osteoclast differentiation [50], circRBM23 and hsa_circ_0006859 regulates the switch between osteogenesis and adipogenesis of MSCs via sponging miR-338-3p and miR-431-5p, respectively [51, 52]. Although intense research into the biological roles of some circRNAs in bone processes of osteoporosis has been detailed, the number of related studies is still limited now, and there remains a need for further research to fulfil the potential of this emerging and highly promising class of regulatory molecules in osteoporosis.

Besides as miRNAs sponges, like the mechanism that the above researches mostly probe into, circRNAs can interact with proteins and function as protein sponges or inhibitors, serve as scaffolds to hold different proteins in close proximity, or recruit proteins to specific subcellular compartments [53]. In this study, we further screened for proteins that could interact with circSTX12 using a biotinylated probe targeting the circSTX12 back-spliced sequence [54]. Our study elucidated the mechanism by which circSTX12 competitively binds to the E3 ubiquitin ligase CBL, thereby reducing the interaction and degradation of MST1 by CBL. The increased MST1 activates the Hippo pathway, which lastly inhibits osteogenic differentiation and promotes the adipogenic differentiation of BMSCs.

The proto-oncogene CBL encodes a RING finger E3 ubiquitin ligase that plays a crucial role in the proteasomal degradation of targeted substrates [55]. It mediates the transfer of ubiquitin from ubiquitin conjugating enzymes (E2) to specific substrates. This protein also contains an N-terminal phosphotyrosine binding domain that allows it to interact with numerous tyrosine-phosphorylated substrates and target them for proteasome degradation [56]. As such it functions as a negative regulator of many signal transduction pathways [57, 58]. It has been reported that CBL is indispensable for regulating osteoblast proliferation, differentiation, survival and apoptosis through the ubiquitination and degradation of receptor tyrosine kinases (RTKs) and other CBL-targeted proteins [58–62]. Moreover, the extinction of CBL expression decreases osteoclast motility, adhesion and resorbing activity by modulating the degradation of Src kinase [63–65]. Our study revealed that CBL can bind and degrade MST1, a tyrosine-phosphorylated substrate and the upstream member of Hippo pathway. In mammals, Hippo pathway consists of MST1/2 and MST1/2's phosphorylated substrate LATS1/2. While YAP is its major downstream mediator of the Hippo pathway. Activation of Hippo pathway results in the inactivation of YAP by LATS1/2-mediated direct phosphorylation. Phosphorylated YAP is sequestered in the cytoplasm. Conversely, dephosphorylation of YAP induces its transport into the nucleus and subsequent interaction with transcription factors, thereby inducing cell biological processes like proliferation, differentiation, organ growth, stem cell self-renewal et al. [66]. It has been reported that YAP promotes osteogenesis and suppresses adipogenic differentiation [67]. In this study, we assessed the underlying mechanisms of circSTX12's role in regulating the MST1 level through post-translational modification of ubiquitination. CircRNAs have been reported to be involved in the regulation of ubiquitination to maintain proteins level. A previous study showed that circMTCL1 binds and increases the C1QBP expression by inhibiting its ubiquitin-proteasome degradation [54]. circNfix binds to YBX1 and promotes its degradation by an E3 ubiquitin ligase Nedd4l [68]. In our study, circSTX12 was found to increase MST1 expression through inhibiting its degradation induced by CBL. CircSTX12 competitively bound to CBL, resulting in reduced ubiquitination and degradation of MST1 by CBL, which in turn inhibited the YAP nuclear signaling and finally promoted adipogenic differentiation and attenuated osteogenic differentiation of BMSCs.

In this study, we investigated the mechanism through which circSTX12 blocks BMSCs proliferation and found that it is related to another protein LMO7. The RNA pull-down assay confirmed that circSTX12 interacts with LMO7. LMO7, or LIM Domain Only 7, is a large protein of 1683 residues that expressed in a variety of tissues and cells [69]. According to previous studies, LMO7 has been linked to Emery-Dreifuss muscular dystrophy (EDMD) by regulating transcription of emerin [70]. Recent research suggests LMO7 coordinates the interaction of many proteins. In vascular smooth muscle cells, LMO7 can interact with c-FOS and c-JUN to promote their ubiquitination and degradation, inhibiting TGF-β signaling and potentially serving as a novel target for regulating fibrotic responses [24]. LMO7 has also long been reported to play a positive role in cell proliferation. For example, it functions as a transcriptional activator controlling myoblast proliferation gene expression [38]. Defects in LMO7 suppress pancreatic cancer cell proliferation and colony formation [71]. Moreover, LMO7 acts to control mitosis progression [72]. Mechanistically, LMO7 mediates signaling between the nucleus and the cytoplasm, sequestering nuclear factors into the cytoplasm and interacting with actin microfilaments [37]. However, little is known about whether LMO7 regulates BMSCs proliferation. Herein, we

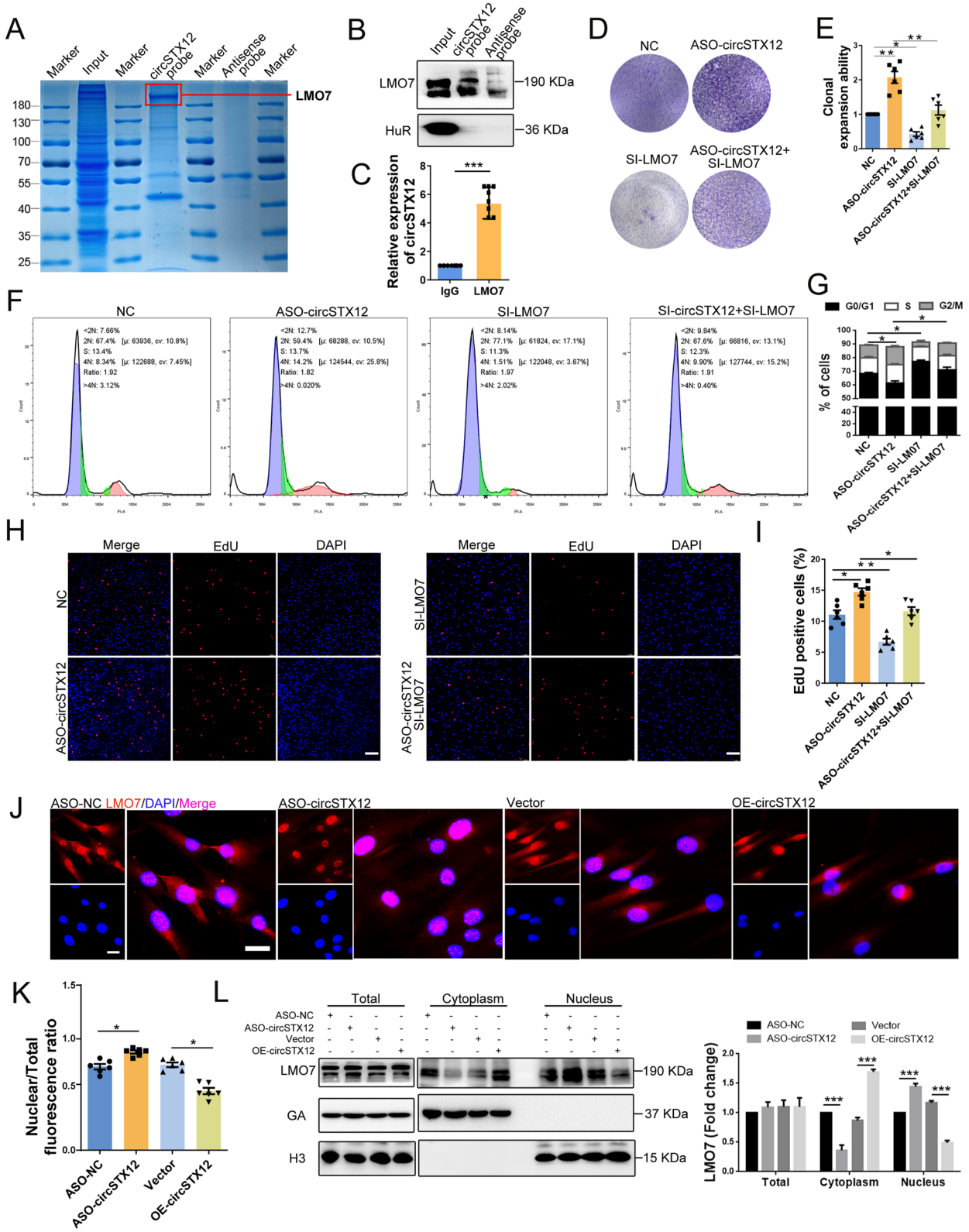
A
Marker
Input
Marker
circSTX12 probe
Marker
Antisense probe
Marker
LMO7
180
130
100
70
55
40
35
25
B
Input
circSTX12 probe
Antisense probe
LMO7
190 KDa
HuR
36 KDa
C
Relative expression of circSTX12
***
IgG
LMO7
D
NC
ASO-circSTX12
SI-LMO7
ASO-circSTX12+ SI-LMO7
E
Clonal expansion ability
NC
ASO-circSTX12
SI-LMO7
ASO-circSTX12+SI-LMO7
F
NC
ASO-circSTX12
SI-LMO7
SI-circSTX12+SI-LMO7
G
G0/G1
S
G2/M
% of cells
NC
ASO-circSTX12
SI-LMO7
ASO-circSTX12+SI-LMO7
H
Merge
EdU
DAPI
NC
ASO-circSTX12
SI-LMO7
ASO-circSTX12 SI-LMO7
I
EdU positive cells (%)
NC
ASO-circSTX12
SI-LMO7
ASO-circSTX12+SI-LMO7
J
ASO-NC LMO7/DAPI/Merge
ASO-circSTX12
Vector
OE-circSTX12
K
Nuclear/Total fluorescence ratio
ASO-NC
ASO-circSTX12
Vector
OE-circSTX12
L
Total
Cytoplasm
Nucleus
ASO-NC
ASO-circSTX12
Vector
OE-circSTX12
LMO7
190 KDa
GA
37 KDa
H3
15 KDa
ASO-NC
ASO-circSTX12
Vector
OE-circSTX12
LMO7 (Fold change)
Total
Cytoplasm
Nucleus

Fig. 7 CircSTX12 binds to and sequesters LMO7 in the cytoplasm. **A.** SDS-PAGE electrophoresis followed by Coomassie brilliant blue staining of the circSTX12-protein complex pulled down by the circSTX12 probe or the antisense probe in protein extracts from BMSCs. The red frame indicates LMO7. **B**. Western blot analysis of LMO7 and HuR levels in BMSCs pulldowns with the circSTX12 probe or antisense probe. **C**. qPCR analysis of circSTX12 after RIP to evaluate the interaction between LMO7 and circSTX12 in BMSCs. $n=8$ biological replicates. **D.** Clonal expansion of BMSCs transfected with NC or ASO-circSTX12 and LMO7 knockdown (SI-LMO7) or not. **E**. Histogram showed the analysis of the clonal expansion of BMSCs in panel D. $n=6$ biological replicates. **F.** Flow cytometry analysis of the cell cycle distribution of BMSCs transfected with NC or ASO-circSTX12 and LMO7 knockdown (SI-LMO7) or not. **G**. Histogram of the percentages of cells in the G0/G1, S, and G2/M phases of the cell cycle, corresponding to panel F. The percentage of cells in different phases was analysed by FlowJo. $n=6$ biological replicates. **H.** EdU staining of BMSCs transfected with NC or ASO-circSTX12 and SI-LMO7 or not after 48 h. Scale bar = 100 μm. **I**. Histogram of the percentage of EdU-positive BMSCs in panel H. $n=6$ biological replicates. **J.** Immunofluorescence staining of LMO7 (red) and DAPI (blue) in BMSCs with circSTX12 knockdown or overexpression. Scale bar (LMO7 and DAPI) = 40 μm. Scale bar (Merge) = 20 μm. **K**. Histogram showed the fluorescence ratio of nuclear/total of LMO7 staining in BMSCs with circSTX12 knockdown or overexpression and the control, corresponding to panel J. $n=6$ biological replicates. **L**. Left panel showed the Western blot results of LMO7 protein levels in total protein, cytoplasmic protein and nucleic protein extracted from BMSCs transfected with ASO-NC, ASO-circSTX12, vector, or OE-circSTX12, respectively. GAPDH was used as a cytoplasmic control, and H3 was used as a nuclear control. Right panel showed the histogram of LMO7 fold change in left panel. $n=6$ biological replicates. All the data are presented as the mean ± SEM. *$p<0.05$, **$p<0.01$, ***$p<0.001$

provided evidence that LMO7 promotes BMSCs proliferation. We found that LMO7 deficiency led to proliferation inhibition in BMSCs and counteracted the pro-proliferative effect after circSTX12 knockdown. LMO7 induced BMSCs proliferation by increasing cyclin A2 (CCNA2), cyclin H (CCNH) and cyclin D1 (CCND1) transcription, suggesting LMO7 as an essential regulator of BMSCs regeneration. Cyclin A2, cyclin H and cyclin D1 belong to the highly conserved cyclin family, whose members are characterized by a dramatic periodicity in protein abundance through the cell cycle. Cyclins bind cyclin-dependent kinases (CDKs) and regulate their enzyme activity, thus helping to drive and coordinate the cell cycle [73]. In the current study, we found for the first time that LMO7 is a pivotal activator for the transcription of CCNA2, CCNH and CCND1 genes through CUT&Tag assay. And the nuclear translocation of LMO7 was regulated by circSTX12 binding. The interaction between circSTX12 and LMO7 prevented nuclear translocation of LMO7, causing LMO7 cytoplasmic retention, thereby reducing the transcription of CCNA2, CCNH and CCND1 genes and inhibiting BMSCs proliferation.

Antisense oligonucleotides (ASOs) are defined as chemically synthesized and modified oligonucleotides, generally 12–30 nucleotides in length, that are designed to bind to RNA by Watson-Crick base pairing rules resulting in RNA degradation by RNase H [74]. The administration of ASOs has emerged as a novel approach to downregulate wild type and mutant transcripts, including miRNAs, lncRNAs, circRNAs et al., and has been successful in the silencing of genes in the central and peripheral nervous system, retina, liver, muscle and bone et al. [75]. There are several approved ASO drugs and a broad pipeline in development. The second and third generation ASOs, which were modified to improved the outcomes and minimize the toxicity from the first generation ASOs, are currently available in the market or are undergoing clinical trials, showing beneficial outcomes in refractory diseases such as amyloidosis, muscular atrophy and lymphoma [76]. Despite this, ASOs have yet to be successfully tested in clinical trials for the treatment of bone-related disease including senile osteoporosis. There have been many attempts in animal studies to use ASOs to improve bone formation. Pei-Ju Tai et al. knock down dickkopf-1 via ASOs to alleviate estrogen deficiency induction of bone loss [77]. Ernesto Canalis et al. use of ASOs to target Notch3 and Notch2 respectively in skeletal cells to ameliorate cortical osteopenia [78, 79]. Feng-Sheng Wang et al. losing of HSP60 signaling by in vivo HSP 60 ASOs treatment contributes to the glucocorticoid-induced enhancement of pro-apoptotic reactions [80]. The injection method of the ASOs in these reports is intravenous application, and the dose is 5–20 nM. In our study, we provide evidence that intravenous treatment of 10 nM chemically modified ASOs formulation targeting circStx12, which improves the proliferation and osteogenic capacity of BMSCs, has a significant effect on alleviating bone loss in aged mice. This strongly supports the value of ASO-based targeting circSTX12 for the treatment of senile osteoporosis.

Taken all together, our data clarify the role of circSTX12 in senile osteoporosis and elucidate the detailed mechanism by which circSTX12 binds to CBL and LMO7 to facilitate osteo-adipogenic balance and the proliferation of BMSCs. Moreover, our findings highlight circSTX12 as an attractive focus and therapeutic target for senile osteoporosis treatment. This study has certain limitations that require further study. We did not explore the exact mechanism for the associations among circSTX12, CBL and MST1. We speculate that the interaction of CBL with circSTX12 might change the conformation of CBL and inhibit the binding of CBL with MST1. Moreover, we did not specifically study the motifs through which circSTX12 interacts with CBL. In addition, the motif involved in the interaction between circSTX12 and LMO7 has not yet been explored. Our hypothesis that cicSTX12 recruits LMO7 proteins to specific subcellular compartments is supported by the results of the nucleoplasmic cell isolation test and immunofluorescence staining. While the exact mechanism that retains LMO7 in the cytoplasm still needs further study. Although attempts have

A

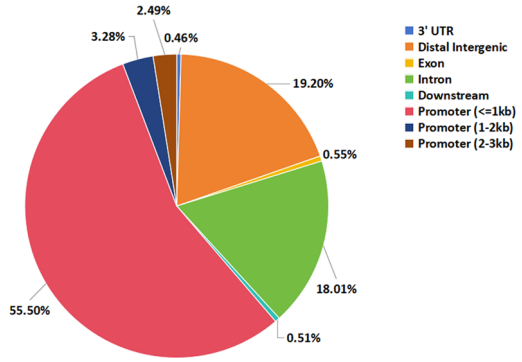

B

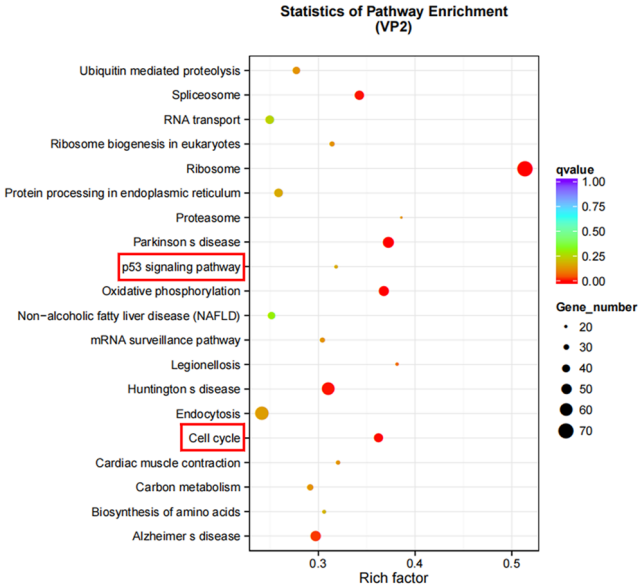

C

CCNA2	SFN	GADD45A	COP1
CCNH	CDC25B	GSK3B	PMAIP1
CCND1	CDC25A	ORC3	PPM1D
CCNG2	BUB3	YWHAZ	SMC1B
RRM2	PIK3R3	AKT3	MAD1L1
PCNA	CUL1		ORC4

D

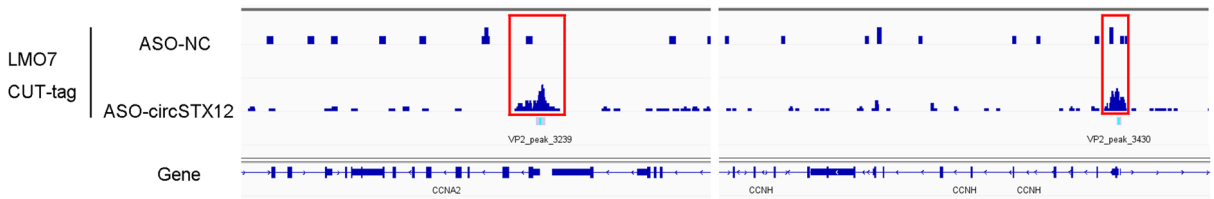

E

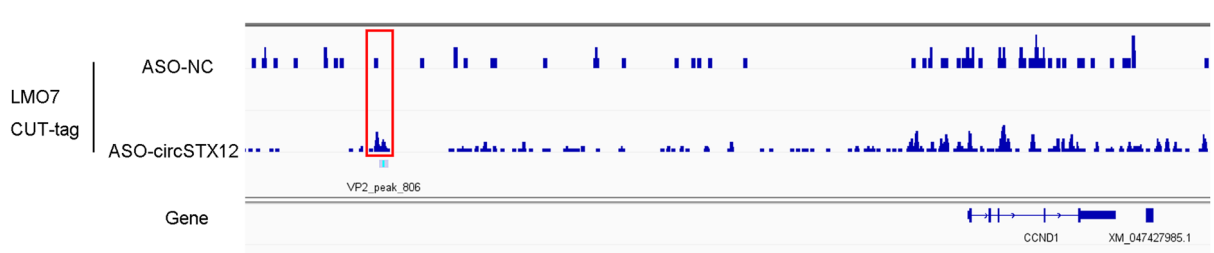

F

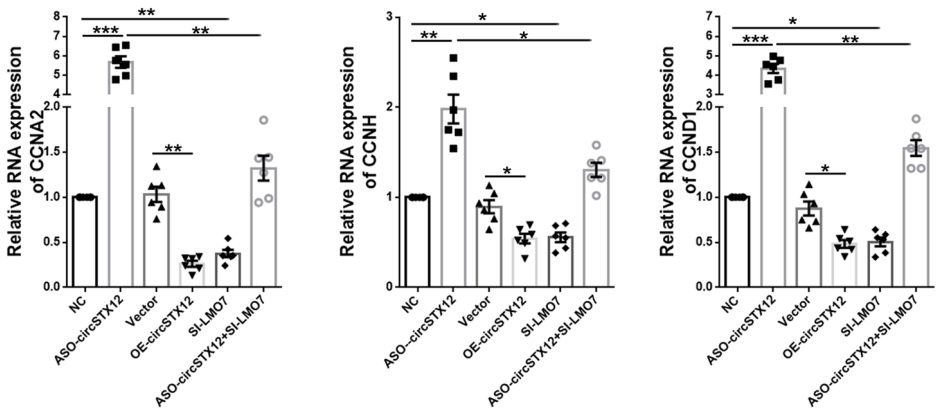

Fig. 8 CircSTX12/LMO7 affects the transcription of CCNA2, CCNH and CCND1. **A.** Pie chart depicted LMO7 peak enrichment percentages in different repeat sequence classes as detected by CUT&Tag-seq. **B**. The top 20 KEGG terms based on the KEGG analysis of the genes with LMO7 peaks in BMSCs after circSTX12 knockdown. VP2 refers to the circSTX12-depleted group. Red frames indicate cell cycle and p53 signaling pathway terms. **C**. The DEGs related to the cell cycle and p53 signaling pathway in the circSTX12-depleted group and the control group. The orange background indicates the upregulated genes, while the green background indicates the downregulated genes. **D**. Genome browser view of LMO7 enrichment peaks (Red frames) at the promoter region of the CCNA2 (left) and CCNH (right) genes in BMSCs infected with ASO-circSTX12 or the control. "VP2_peak_3239" means the peak number (NO.) is 3239 in circSTX12-depleted group in the LMO7 CUT&Tag-seq. "VP2_peak_3430" means the peak NO. is 3430 in circSTX12-depleted group in the LMO7 CUT&Tag-seq. **E**. Genome browser view of LMO7 enrichment peak (Red frame) at the distal intergenic region of the CCND1 gene in BMSCs infected with ASO-circSTX12 or the control. "VP2_peak_806" means the peak NO. is 806 in circSTX12-depleted group in the LMO7 CUT&Tag-seq. **F**. qPCR results of CCNA2, CCNH and CCND1 in BMSCs transfected with NC or ASO-circSTX12, with or without SI-LMO7, or with the circSTX12 overexpression or the control for 2 days. NC was the control of both ASO-circSTX12 and SI-LMO7 groups. Vector was the control of the OE-circSTX12 group. $n=6$ biological replicates. All the data are presented as the mean ± SEM. *$p<0.05$, **$p<0.01$, ***$p<0.001$

been made to transport ASOs to bone specifically, further research of complex delivery systems of ASOs specific to bone are still necessary [81]. Overall, our findings provide novel insights into the relationship between circSTX12 and BMSCs differentiation and proliferation while highlighting the therapeutic potential of ASO-circSTX12 for age-related osteoporosis treatment in vivo.

Materials and methods

Ethics statement

This study was approved by the Ethics Committee of the Eighth Affiliated Hospital Sun Yat-sen University, Shenzhen, China (Approval No. 2022-084-01). All patients and volunteers were made aware of the study procedures and potential risks, and informed consent was obtained. Animal experiments were reviewed and approved by the Institutional Animal Care and Use Committee (IACUC), Sun Yat-Sen University (SYSU-IACUC-2022-002487). All the experiments performed in this study were conducted in accordance with the committee's regulations and guidelines.

Isolation and culture of BMSCs

All the participants signed informed consent forms. The experimental protocol was approved by the institutional ethics committee of The Eighth Affiliated Hospital of Sun Yat-sen University. Bone marrow aspirates (10–20 ml) from each donor were seeded in 5-cm^2 flasks containing medium (DMEM (HyClone, USA), 10% foetal bovine serum (Gibco, USA), 100 U/ml penicillin G and 100 mg/ml streptomycin [HyClone, USA]) in a cell incubator at 37 °C. After 3–5 days of culture, the supernatant and non-adherent cells were removed. The attached cells were detached with 0.25% trypsin (Gibco, USA) and reseeded into new 75 cm^2 flasks. BMSCs at passages 3–5 were used for the experiments on differentiation and proliferation.

Collection of human bone samples

Osteoporosis samples from patients with aging osteoporosis who underwent surgery were collected. Osteopenia group as well as normal control samples from patients who underwent surgery after an accident were acquired. T-score evaluated after a dual energy X-ray absorptiometry (DXA) examination on the lumbar spine was taken as criterion to classify the populations into three groups: young control group (healthy donor, $n=11$, mean age = 22.5 ± 3.8 y), osteopenia group ($n=9$, mean age = 55.4 ± 2.9 y, mean T-score = -1.70 ± 0.50) and osteoporotic group ($n=10$, mean age = 76.0 ± 7.8 y, mean T-score = -2.59 ± 0.30). After obtaining informed consent, we acquired the bone tissues. Sections and protein of bone tissue of different groups were acquired. BMSCs of different groups were isolated.,

Adipogenic and osteogenic differentiation of BMSCs

BMSCs were seeded at $0.5–0.8\times10^5$ cells/well in 12-well plates, and the osteogenic medium (DMEM supplemented with 10% FBS, 100 IU/ml penicillin, 100 IU/ml streptomycin, 0.1 mM dexamethasone, 10 mM β-glycerol phosphate, and 50 mM ascorbic acid (Sigma-Aldrich, St. Louis)) was replaced every 3 days. For adipogenic induction, BMSCs were induced in adipogenic medium (high-glucose DMEM supplemented with 10% FBS, 1 mM dexamethasone (Sigma-Aldrich), 10 mg/ml insulin (Sigma-Aldrich), 0.5 mM 3-isobutyl-1-methylxanthine (Sigma-Aldrich), and 0.2 mM indomethacin (Sigma-Aldrich)), with the medium replaced every 3 days.

ALP, ARS and ORO staining and quantification

For alkaline phosphatase (ALP) staining, BMSCs, osteogenically differentiated for 7 days, were fixed in 4% formaldehyde, stained using a BCIP/NBT alkaline phosphatase kit (Beyotime Institute of Biotechnology) in accordance with the manufacturer's instructions, and then imaged using a Nikon TS-2 microscope. For the ALP activity assay, ALP activity kits (Nanjing Jiancheng Biotech) were used in accordance with the manufacturer's instructions. Briefly,

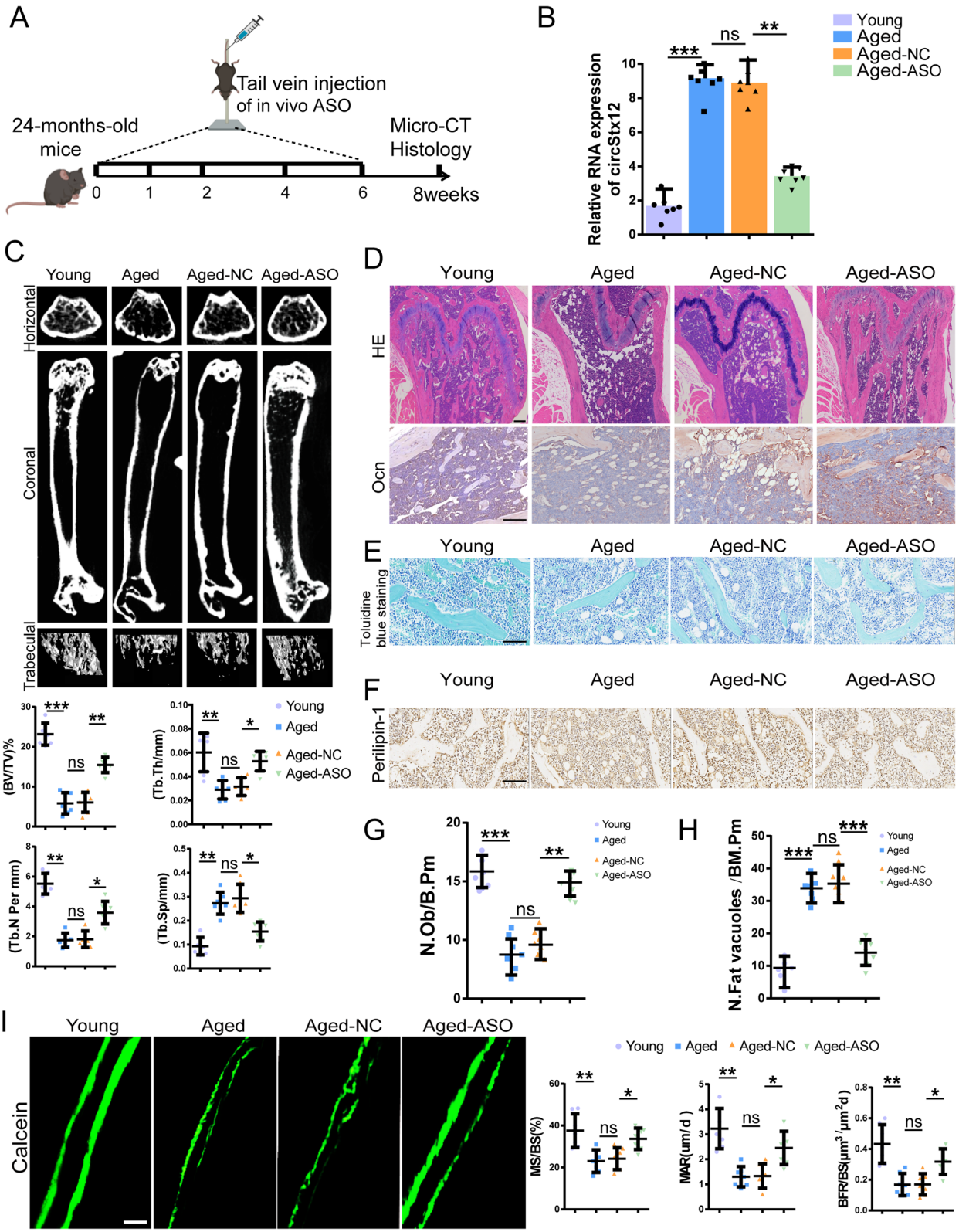
A
Tail vein injection
of in vivo ASO
24-months-old
mice
Micro-CT
Histology
0
1
2
4
6
8weeks
B
Young
Aged
Aged-NC
Aged-ASO
Relative RNA expression
of circStx12
***
ns
**
C
Young
Aged
Aged-NC
Aged-ASO
Horizontal
Coronal
Trabecular
(BV/TV)%
(Tb.Th/mm)
(Tb.N Per mm)
(Tb.Sp/mm)
D
HE
Ocn
E
Toluidine
blue staining
F
Perilipin-1
G
N.Ob/B.Pm
H
N.Fat vacuoles /BM.Pm
I
Calcein
MS/BS(%)
MAR(um/d)
BFR/BS(μm³/μm²d)

Fig. 9 Silencing of circStx12 suppresses OP pathogenesis in a mouse model. **A.**Schematic of the time course of the experiments in (B-E). **B.** RT-qPCR showed the level of circStx12 in the bone tissues of saline-injected 6-month-old mice (Young), saline-injected 24-month-old mice (Aged), control ASO-injected 24-month-old mice (Aged-NC), 10 nM circStx12-ASO-injected 24-month-old mice (Aged-ASO). **C**. Micro-CT analysis of femurs from mice in different groups in panel B. The 3D trabecular bones were reconstructed. Bone morphometric analysis was performed, and the parameters included bone volume/total volume (BV/TV), trabecular thickness (Tb.Th), trabecular number (Tb.N) and trabecular space (Tb.Sp). **D**. H&E and Ocn staining of femurs from mice in different groups. Scale bar = 500 μm (H&E), Scale bar = 250 μm (Ocn). **E**. Representative images of toluidine blue staining of femurs from mice in different groups. Scale bar = 250 μm. **F.** Perilipin-1 immunohistochemical staining of femurs from mice in different groups. Scale bar = 250 μm. **G.** Quantification of the number of osteoblasts per bone perimeter (N.Ob/B.Pm) were evaluated via "osteomeasure." **H.** Quantification of the number of adipocytes per bone marrow perimeter(N.Fat vacuoles /BM.Pm). **I.** Calcein green double staining of femurs from mice in different groups. Scale bar = 20 μm. Dynamic reconstruction parameters include the mineralized surface/bone surface area (MS/BS), mineral accumulation rate (MAR), and bone formation rate/bone surface (BFR/BS). The data are shown as the mean ± SEM. $n = 7$ biological replicates. *$p < 0.05$, **$p < 0.01$, ***$p < 0.001$, ns: no significance

BMSCs osteogenically differentiated for 7 days were lysed using RIPA buffer, the supernatants were incubated with reaction buffer for 15 min, and then stop solution was added. The absorbance was measured at 405 nm. The total protein concentration was detected by a bicinchoninic acid (BCA) protein assay kit (Thermo Fisher Scientific). ALP activity was normalized to the total protein content and reported as units per gram of protein per 15 min (U/g pro/15 min).

For Alizarin Red S (ARS) staining, BMSCs cultured in osteogenic medium for 14 days were first fixed in 4% paraformaldehyde for 30 min and then stained with 1% ARS (A5533, Sigma-Aldrich, pH 4.3) for 30 min at room temperature. After being washed at least three times with phosphate-buffered saline (PBS), the stained cells were observed and photographed under a Nikon TS-2 microscope. Then, the cells were destained with 10% cetylpyridinium chloride monohydrate (Sigma-Aldrich) for 1 h at room temperature; 200 μL of the extracted liquid was transferred to a 96-well plate, and the absorbance was measured at 562 nm.

For Oil Red O (ORO) staining, BMSCs subjected to adipogenic induction for 14 days were fixed with 4% paraformaldehyde for 30 min. Then, ORO working solution (O0625, Sigma-Aldrich, 10 mg/ml) was added and incubated with the fixed cells for 20 min at room temperature. The stained cells were observed under a microscope. Quantitative analysis was performed by extraction with isopropanol and subsequent measurement of the absorbance at 520 nm.

ASOs transfection in vitro

In the circSTX12 ASO group, 1.0×10^5 BMSCs were transfected with circSTX12 ASO (50 nM) or control ASO (NC) when cell confluence reached 60 to 80%. The circSTX12 ASO sequence (3'-GAAGUCUUGUCGACGAGUCU-5') and the NC sequence were designed and synthesized by Guangzhou Ruibo Biological Co., Ltd.

RNA interference

Small interfering RNAs (siRNAs) targeting CBL and LMO7 and negative controls were purchased from IGEbio (Guangzhou, China). When cell confluence reached 60 to 80%, BMSCs were transfected with Lipofectamine™ RNAiMAX (Invitrogen) and siRNA cocktail (1 OD/1.8×10^6 cells) in Opti-MEM reduced serum medium according to the manufacturer's instructions. qPCR was detected to test the level of the targeted RNAs 48 h after transfection. The siRNA with the highest knockout rate was used in the followed experiments. The sequences of these siRNAs are shown in Supplementary Table 1.

Plasmid construction and transfection

Expression plasmid pLC5-ciR-circSTX12 was constructed by Geneseed (Guangzhou, China). pcDNA3.4(+)-MST1 were constructed by IGE Biotechnology (Guangzhou, China). Transfection was performed using a Lipofectamine 3000 Transfection Kit (Invitrogen, MA, USA) according to the manufacturer's instructions with minor modifications. Briefly, P4 BMSCs were seeded in 12-well plates at a density of 0.8×10^5 cells/well. A total of 0.5 μg plasmid supplemented with 1 μg Lipofectamine 3000 (Thermo Scientifc™) and 1 μg p3000 (Thermo Scientifc™) mixed in Opti-MEM (Gibco) was added to each well. 8 h after transfection, the culture medium was replaced.

YAP inhibitor treatment

BMSCs of passge 4 were seeded in 12-well plates at a density of $0.5–0.8 \times 10^5$ and treated with different concentrations (1.25, 2.5, and 5nM) of YAP Inhibitor (MCE, Italy) dissolved in the osteogenic or adipogenic medium for 14 days. After 14 days, the BMSCs was observed under a microscope and ARS or ORO staining assays were performed followed the above intruduction.

RNA extraction, reverse transcription, and quantitative realtime PCR

Total RNAs were extracted from tissues or cells using TRIzol reagent (Thermo Fisher, USA). RNAs from nucleus and cytoplasm of BMSCs were separated by the PARIS™ Kit (Life Technologies, USA) following the manufacturer's instructions. The purity and concentration of the RNA were spectrophotometrically analysed using a NanoDrop One (Thermo Fisher, USA). To determine the expression levels of circRNAs, 4 U/μg of RNase R (Beyotime, China) was added to digest linear transcripts. cDNA was transcribed using the PrimeScript RT reagent kit (TaKaRa, Japan). To determine mRNA expression, cDNA was transcribed using a First Strand cDNA Synthesis Kit (Beyotime, China). PCR was performed on an ABI 7500 Real-Time PCR system (Thermo Fisher, USA) using TB Green Premix Ex Taq II (Taraka, Japan). GAPDH was used as the reference gene for mRNAs or circRNAs in cell extracts. The primers shown in Supplementary Table 2 were utilized for qPCR.

Protein extraction

The cells were washed three times with PBS and then lysed in RIPA buffer (CWBIO, Jiangsu, China) supplemented with protease inhibitors (CWBIO) and phosphatase inhibitors (CWBIO) for 30 min on ice. Total protein was acquired by centrifuging the lysates at 14,000 rpm for 10 min at 4 °C. The soluble material was collected, and the protein concentration was measured using a Pierce BCA protein assay kit (Thermo Scientific™). Nuclear and cytoplasmic proteins were separated with NE-PER™ Nuclear and Cytoplasmic Extraction Reagents (Thermo Scientific™) according to the manufacturer's instructions, and protein concentrations were determined as described above.

Western blot

Equal amounts of protein samples were diluted with 5 × SDS-PAGE Sample Loading Buffer (Beyotime, P0015) and subsequently transferred to polyvinylidene difluoride (PVDF) membranes (Merck Millipore, IPVH00010). Then, the membranes were transferred to Tris-buffered saline with Tween (TBST) (10 mM Tris-HCl, 15 mM NaCl, 0.05% Tween-20, pH 7.5) solution and washed three times. Afterwards, the membranes were blocked with 5% skim milk (Wako, 190-12865), incubated for 60 min at room temperature, and then incubated with primary antibodies against GAPDH (CST, 5174 S, 1:1000), CBL (Abcam, ab32027, 1:1000) osteocalcin (OCN; Abcam, ab133612, 1:1000), RUNX2 (CST, 12556 S, 1:1000), OSX (Abcam, ab209484, 1:1000), YAP (Affinity Biosciences, DF3182-200, 1:1000), phospho-YAP (Biorigin, BN42106R, 1:1000), LATS1 (SAB, C36187, 1:1000), BMP2 (Abcam, ab284387, 1:1000), Wnt1 (Abcam, Wnt1, #63934, 1:1000), Gli (SAB, 49399-1, 1:1000), Gli2 (SAB, 29217, 1:1000), MST1 (CST, bs-8477R1:1000), β-Catenin (ABclonal, A19657, 1:1000), p-Smad1/Smad5/Smad8 (SAB, 21684, 1:1000), OPN (SAB, 42036, 1:1000), Osteocalcin (Abcam, ab93876, 1:1000), FABP4 (Abcam, ab92501, 1:1000), CEBPA (Abcam, ab40764, 1:1000), PPARG (Abcam, ab178860, 1:1000), and Ubiquitin (Abcam, 134,953, 1:1000) overnight in a 4 °C refrigerator. After washing three times with TBST, horseradish peroxidase (HRP)-conjugated goat anti-mouse IgG (ComWinBiotech, cw0102s, 1:3000) or goat anti-rabbit IgG (ComWin Biotech, cw0103s, 1:3000) secondary antibodies were added and incubated for 60 min at room temperature on a shaker. Finally, the membranes were washed three times with PBS, and the immunoreactive protein bands were detected with Immobilon Western Chemiluminescent HRP Substrate (Merck Millipore, WBKLS0500). Relative quantitative analysis was performed by ImageJ software.

RNA pulldown and mass spectrometry

To identify the proteins that interact with circSTX12, an RNA pull-down assay was performed. Biotin-labelled oligonucleotide probes (CTTTATCTGAGCAGCTGTTC-/3bio/) and antisense probes (GAACAGCTGCTCAGATAAAG-/3bio/) targeting circSTX12 ligation sites for RNA pulldown and mass spectrometry were synthesized by RiboBio (Guangzhou, China). RNA pull-down assays were performed with the PureBindingTM RNA-protein pull-down kit (Geneseed) according to the manufacturer's protocol. Briefly, streptavidin-coated magnetic beads were incubated with biotinylated probes for 1 h at 4 °C. Afterwards, the beads were separated using magnets and incubated with the lysate from 1.0×10^7 BMSCs (in lysis buffer) for an additional 2 h at 4 °C. The probe-RNA-protein complex was pulled down and separated using a magnet. Proteins in the complexes were separated from the magnetic beads by boiling for 10 min and then subjected to Western blot or mass spectrometry (Medical Research Center, Sun Yat-sen Memorial Hospital, Sun Yat-sen University, Guangzhou, China).

RNA Immunoprecipitation (RIP) assay

Interactions between CBL, LMO7 and circSTX12 were detected with an RNA immunoprecipitation kit (Geneseed, Guangzhou, China) applied according to the manufacturer's instructions. Briefly, 2×10^7 cells were collected, lysed with RIP lysis buffer, and then incubated with IgG-conjugated magnetic beads (Cell Signaling Technology, Beverly, MA,

USA) or antibodies against CBL or LMO7. Coprecipitated RNA was detected by RT-qPCR. The sequences of the primers used are listed in Supplementary Table 1.

Coimmunoprecipitation

BMSCs or HEK293T cells were quickly harvested and homogenized on ice in modified RIPA buffer (Beyotime biotechnology). The cell extracts (approximately 200 μg of total protein) were incubated with antibodies against CBL (Abcam, ab32027, 1:1000), MST1 (CST, bs-8477R, 1:1000), or their IgG controls (Cell Signaling Technology, 3452 or 37988) at 4 °C overnight. Then, protein-G agarose beads (40 L, Beyotime Biotechnology) were added, and the mixture was incubated at 4 °C for 3 h. The agarose beads were collected, washed, and resuspended in 60 μL of sample buffer containing 50 mM Tris-HCl, pH 7.6, 2% (wt/vol) SDS, 10% (vol/vol) glycerol, 10 mM DTT, and 0.2% bromophenol blue. Then, the samples were boiled for 10 min. SDS-PAGE was used to separate the samples. The Western blot protocols used are described above. A special secondary antibody (1:1000, Abcam, ab131366) that recognizes only native (nonreduced) antibodies to minimize the detection of heavy and light chains was used to test the IP samples to avoid the influence of the IP antibodies.

RNA fluorescence in situ hybridization (FISH)

RNA FISH was performed with the Fluorescent in Situ Hybridization Kit (RiboBio, Guangzhou, China) according to the manufacturer's instructions. First, BMSCs were seeded in 12-well plates, covered with sterile glass, and cultured overnight. Then, the cells were fixed with 4% paraformaldehyde for 10 min and permeabilized with cold 0.5% Triton for another 5 min. After being rinsed 3 times, the BMSCs were prehybridized with prehybridization buffer for 30 min at 37 °C. A Cy3-labelled circSTX12 probe (TATCTGAGCAGCTGTTCTGAAGTAG) was constructed by Geneseed (Guangzhou, China). The probe was dissolved in hybridization buffer at 20 μM. Then, the slides were hybridized in hybridization buffer overnight. After sequential washes to remove the unconjugated probe, the cells were stained with 4′,6-diamidino-2-phenylindole (DAPI) and observed under an LSM 880 laser scanning confocal microscope.

H_2O_2induced senescence

BMSCs of passage 4 were seeded in 12-well plates at a density of 0.7×10^5 cells/well. Then, the cells were treated with 600 μM H_2O_2 for 2 h to induce senescence. Subsequent experiments were performed on day 7 after induction.

5-Ethyl-2′-deoxyuridine (EdU) incorporation assay

BMSCs of passage 4 were seeded in 24-well plates at a density of 0.4×10^5 cells/well. BMSCs were transfected with siRNAs, ASOs or plasmids and then evaluated for proliferation. Two days after transfection, the cells were observed by fluorescence microscopy. A BeyoClick™ EdU Cell Proliferation Kit (Beyotime) was used according to the manufacturer's protocol. EdU-positive cells were identified and counted using ImageJ software 1.4.

Clonal expansion assay

BMSCs of passage 4 were seeded at a density of 0.4×10^4 cells per well in 12-well plates. Cultures were continued for 10 days with ASOs, siRNAs or plasmids transfection. The cells were then fixed with 4% paraformaldehyde for 10 min and stained with 0.2% crystal violet (Beyotime) for 1 h at room temperature. Clonal expansion was scored using ImageJ 1.4 software.

CUT&tag assay

A NovoNGS® CUT&Tag 2.0 High-Sensitivity Kit (for Illumina®) (Novoprotein Scientific, Inc., Cat# N259-YH01-01 A) was used to perform the CUT&Tag assay. Briefly, cells were harvested and enriched with ConA magnetic beads. A total of 50 000 cells were resuspended and washed twice with 100 μL of Dig-Wash Buffer. The samples were incubated with anti-LMO7 primary antibody (1:100, 4 °C, 18 h) and secondary antibody (1:200, 25 °C, 1 h). After incubation, the beads were washed three times in Dig-Hisalt Buffer. The cells were incubated with protein A-Tn5 transposome at 25 °C for 1 h and washed three times in Dig-Hisalt buffer. The cells were resuspended in 50 μL of tagmentation buffer and incubated at 37 °C for 1 h, and then the reaction was terminated with 1 μL of 10% SDS at 55 °C for 10 min. Phenol chloroform was used to extract the DNA fragments [82].

CUT&Tag sequencing and analysis

The libraries were sequenced on an Illumina NovaSeq 6000 platform at Novogene Science and Technology Co., Ltd. (Beijing, China), which generated PE150 sequencing data. TrimGalore (v0.6.6) was used to filter the sequencing adaptors and low-quality reads with the following parameters: -q 20 --phred33 --stringency 3. Bowtie2 (v2.5.1)52 was used to map clean reads to the genome with the default parameters. MACS2 (v.2.1.1)55 was used to call peaks with the following parameters: -q 0.05 --call-summits --nomodel–shift −100 --extsize 200 --keep-dup all. The computeMatrix and

plotHeatmap commands in deepTools (v2.3.6.0)56 were used to plot heatmaps of the CUT&Tag data [82].

Animal models

Male C57BL/6J mice were obtained from the Animal Experimental Center of Sun Yat-sen University. 24-month-old (aged) mice and 6-month-old (young) mice were prepared and kept in the experimental environment for at least 1 week prior to additional treatment. The mice were housed under controlled environmental conditions (23 ± 1 °C; 50–60% humidity) with a 12: 12 h light: dark cycle and free access to food and water.

ASOs in vivo treatment experiment

For the ASOs in vivo treatment experiment, we first conducted a preliminary experiment. Aged mice were randomized into 4 groups (3 mice in each group). ASOs (0, 5, 10, and 15 nM) in 100 µl of saline were delivered through tail vein injection at weeks 0, 1, 2, 4, and 6 for a total of 5 injections. Femur samples were harvested at week 8. The group of 15 nM of circStx12 ASO use in mice was excluded from the followed analysis, for one mouse died one day after the first injection and two died one day after the second injection, indicating the toxicity of the 15 nM dose in vivo. Tail-intravenous injection of 10 nM of ASOs caused 60-70% down-regulation of circStx12 even after 2 weeks in femur without toxicity in vivo. While 5 nM of ASOs caused only ~ 10% down-regulation of circStx12 in vivo. Then the dose of 10 nM ASO was chosen for the subsequent expanded sample size experiment ($n = 7$ mice per group). Four groups of mice were assessed in this study: the saline-injected 6-month-old (Young) group, the saline-injected 24-month-old group (Aged), the control ASO-injected 24-month-old group (Aged-NC), and the circSTX12-ASO-injected 24-month-old group (Aged-ASO). Ten and three days before sample harvesting, calcein (10 µg/g) was intraperitoneally injected, and at week 8, the bone tissue, primary organ and BMSCs samples were harvested, and bone static and dynamic histomorphometry were assessed [83]. The circStx12 ASOs sequence was designed and synthesized by Guangzhou Ruibo Biological Co., Ltd.

Bone tissue staining

Mice femurs were fixed in 4% paraformaldehyde for 36 h and decalcified with EDTA-decalcifying fluid (BOSTER, AR1071) for 3 weeks. Afterwards, paraffin embedding was performed, and 5-µm sections were stained with H&E. The sections were dewaxed in xylene, rehydrated in gradient ethanol, and then rinsed in distilled water. For H&E staining, sections were stained in haematoxylin for 8 min. The samples were rinsed with running water and dehydrated in 70% and 90% alcohol for 10 min each. Subsequently, the femur sections were stained with alcohol eosin for 3 min.

For OCN immunohistochemical staining, after rehydration, the slides were immersed in 10 mM citrate buffer (pH 7.5) and microwaved at 750 W for 30 min for antigen retrieval. Then, the samples were treated with 3% H_2O_2 for 20 min, blocked with 5% normal goat serum for 1 h at room temperature, and stained with rabbit anti-OCN primary antibody (Abcam, ab133612, 1:200) and the fat vacuoles were stained with a Perilipin-1 antibody (Cell Signaling Technology Cat# 9349,1:100) in blocking buffer overnight at 4 °C. Pure donkey anti-rabbit IgG antibody (Jackson ImmunoResearch, USA, Cat# 711-225-152) was used as a secondary antibody (1:200). After being extensively washed with PBS, the slides were stained with standard DAB for chromogenic detection via immunohistochemistry. After staining, all sections were dehydrated with increasing concentrations of ethanol and xylene. Images were taken and analysed using a Leica DMi8 microscope.

For immunofluorescence staining, the BMSCS was seeded seeded in 12-well plates, covered with sterile glass, and cultured overnight. Then, the cells were fixed in 4% paraformaldehyde for 30 min, permeabilized by 0.1% Triton X-100 for 15 min at room temperature, and then blocked by 5% normal goat serum for 30 min. Then the BMSCs or the sections were incubated with primary antibodies against YAP (Affinity Biosciences, DF3182-200, 1:1000) overnight at 4℃, respectively. Then the BMSCs or sections were stained with fluorophore-conjugated secondary antibodies and mounted with DAPI in anti-fade mounting medium (Thermo Fisher Scientific, Cat# S36963). Images were taken and analysed using a Leica DMi8 microscope.

For Toluidine blue staining, soak the slices in 0.5% toluidine blue staining solution for 30 min. Then rinse with water slightly to remove excess dye. Subsequently, differentiation is carried out using glacial acetic acid solution, which can be prepared in a ratio of 0.5-1:100 with distilled water. The differentiation time depends on the staining effect, usually ranging from a few seconds to a few minutes, until the nuclei and particles are clear. After slightly washing with water, dry the slices with cold air. Finally, use xylene for transparency treatment and seal with neutral gum. Images were taken and analysed using a Leica DMi8 microscope. The number of Osteoblasts (N.Obs) were evaluated on Osteomeasure Software (OsteoMetrics, Decatur, USA).

For tartrate-resistant acid phosphatase (TRAP) staining, after the sections were dewaxed to water, TRAP staining solution was added and incubated at 37 ℃ for 30–60 min. Rinse with distilled water, lightly stain the nucleus with hematoxylin for 3–5 min, and then rinse with distilled water

to return to blue. The tissue sections were sealed with a neutral gum after dehydration and transparency. Images were taken and analysed using a Leica DMi8 microscope. The number of osteoclasts (N.Ocs) were evaluated on Osteomeasure Software (OsteoMetrics, Decatur, USA).

Microcomputed tomography (micro-CT) and histomorphometric analyses

Mice femurs were dissected, fixed in 4% paraformaldehyde for 36 h, and stored in 70% ethanol. The samples were scanned using a Siemens mCT40 scanner (Siemens, Germany) at 55 kV/70 mA and a Siemens 1275 mCT imaging system (Siemens, Germany) following the guidelines for the assessment of bone microstructure in rodents. For trabecular bone analysis, the regions of interest were defined as the areas 0.5 mm proximal to the growth plate in the distal femurs. Two- and three-dimensional bone structure images were reconstructed. To examine the rate of bone formation, mice were injected intraperitoneally with 10 mg/kg calcein (Sigma–Aldrich, Cat# T3383) dissolved in PBS on day 10 and day 3 before harvesting the samples. Femurs were collected and fixed in 4% paraformaldehyde for 36 h, and undecalcified bone slices (8 mm) were obtained. The mineralized surface/bone surface area (MS/BS), mineral apposition rate (MAR) and bone formation rate (BFR) were measured as previously described [84].

Statistical analysis

Each experiment was repeated three times. All the data are expressed as the mean ± SEM. Statistical analysis was performed using GraphPad Prism 7.0. Student's t test was used to test the difference between two groups. One-way analysis of variance (ANOVA) was used to test differences between three or more groups. Receiver operating characteristic (ROC) analysis was performed to evaluate the diagnostic (disease prediction) ability of gene expression. Differences were considered statistically significant when $p < 0.05$.

Supplementary Information The online version contains supplementary material available at https://doi.org/10.1007/s00018-025-05684-y.

Acknowledgements The authors thank American Journal Experts for providing English language editing of the manuscript and Medpeer for providing help for the schematic diagram.

Author contributions Conceptualization, Y.W., H.S. S.W. and W.Y.; Methodology and Software, H.G. and S.W.and Z.W.; Validation, S.W., H.G., and F.C; Formal Analysis and Investigation, P.F. and C.Z.; Data Curation, W.Y. Q.C. and H.G.; Writing-Original Draft Preparation, S.W.and H.G.; Writing-Review & Editing, H.G., Y.W.; Supervision, H.S; Project Administration, Y.W.; Resources and Funding Acquisition, H.S., S.W., and Y.W. All authors approved the final manuscript.

Funding This study was supported by the Basic and Applied Basic Research Foundation of Guangdong Natural Science Foundation(2024A1515010930), Shenzhen Science and Technology Planning Project (NO. JCYJ20220530144017040), the Futian Healthcare Research Project (No.FTWS2022075) and the National Natural Science Foundation of China (82172385, 82172349).

Data availability The data used to support the findings of this study are included within the article and the supplementary materials, and are available from the corresponding author upon request.

Declarations

Ethics approval and consent to participate The study was conducted in accordance with the Declaration of Helsinki and approved by the Ethics Committee of the Eighth Affiliated Hospital of Sun Yat-sen University. All of the participants signed informed consent forms.

Consent for publication Informed consent was obtained from all subjects involved in the study.

Competing interests No competing financial interests exist.

References

1. Wang H et al (2020) Mechanistic advances in osteoporosis and anti-osteoporosis therapies. MedComm 2023. 4(3): p. e244
2. Li J et al (2020) The relationship between bone marrow adipose tissue and bone metabolism in postmenopausal osteoporosis. Cytokine Growth Factor Rev 52:88–98
3. Hoover MY et al (2023) Purification and functional characterization of novel human skeletal stem cell lineages. Nat Protoc 18(7):2256–2282
4. Qadir A et al (2020) Senile osteoporosis: the involvement of differentiation and senescence of bone marrow stromal cells. Int J Mol Sci, 21(1)
5. Lee JE et al (2020) MLL3/MLL4-Associated PAGR1 regulates adipogenesis by controlling induction of C/EBPβ and C/EBPδ. Mol Cell Biol, 40(17)
6. Xu F et al (2020) The roles of epigenetics regulation in bone metabolism and osteoporosis. Front Cell Dev Biol 8:619301
7. Pérez-Campo FM et al (2016) Osterix and RUNX2 are transcriptional regulators of sclerostin in human bone. Calcif Tissue Int 99(3):302–309
8. Dang F, Nie L, Wei W (2021) Ubiquitin signaling in cell cycle control and tumorigenesis. Cell Death Differ 28(2):427–438

9. Chen F et al (2023) Silencing circSERPINE2 restrains mesenchymal stem cell senescence via the YBX3/PCNA/p21 axis. Cell Mol Life Sci, 80(11)
10. Shoji H, Miyakawa T (2019) Age-related behavioral changes from young to old age in male mice of a C57BL/6J strain maintained under a genetic stability program. Neuropsychopharmacol Rep 39(2):100–118
11. Mazziotta C et al (2024) Regulatory mechanisms of circular RNAs during human mesenchymal stem cell osteogenic differentiation. Theranostics 14(1):143–158
12. Chen R et al (2023) Engineering circular RNA for enhanced protein production. Nat Biotechnol 41(2):262–272
13. Lin Z et al (2021) Functions and mechanisms of circular RNAs in regulating stem cell differentiation. RNA Biol 18(12):2136–2149
14. Wang CC et al (2021) Circular RNAs and complex diseases: from experimental results to computational models. Brief Bioinform, 22(6)
15. Luo Y et al (2021) Circular RNAs in osteoporosis: expression, functions and roles. Cell Death Discov 7(1):231
16. Liu X et al (2022) Circular RNA: an emerging frontier in RNA therapeutic targets, RNA therapeutics, and mRNA vaccines. J Control Release 348:84–94
17. Zhang D et al (2021) CircRNA-vgll3 promotes osteogenic differentiation of adipose-derived mesenchymal stem cells via modulating miRNA-dependent integrin A5 expression. Cell Death Differ 28(1):283–302
18. Huang Y et al (2020) Circular RNA YAP1 attenuates osteoporosis through up-regulation of YAP1 and activation of Wnt/β-catenin pathway. Biomed Pharmacother 129:110365
19. Yang Y et al (2020) The roles of MiRNA, LncRNA and circrna in the development of osteoporosis. Biol Res 53(1):40
20. Li S et al (2019) Microarray is an efficient tool for circrna profiling. Brief Bioinform 20(4):1420–1433
21. 342 (2021) Role and mechanism of action of circular RNA and laryngeal cancer. Pathol Res Pract 223:153460
22. Zhou WY et al (2020) Circular RNA: metabolism, functions and interactions with proteins. Mol Cancer 19(1):172
23. Wang S et al (2022) RNA sequencing reveals the expression profiles of circrnas and indicates Hsa_circ_0070562 as a Pro-osteogenic factor in bone Marrow-Derived mesenchymal stem cells of patients with ankylosing spondylitis. Frontiers in Genetics, p 13
24. Li J et al (2019) TRAF4 positively regulates the osteogenic differentiation of mesenchymal stem cells by acting as an E3 ubiquitin ligase to degrade Smurf2. Cell Death Differ 26(12):2652–2666
25. Li J et al (2020) GAS5 protects against osteoporosis by targeting UPF1/SMAD7 axis in osteoblast differentiation. eLife, 9
26. Xiang L et al (2018) The versatile Hippo pathway in oral-maxillofacial development and bone remodeling. Dev Biol 440(2):53–63
27. Ren W et al (2020) Changes of WNT/B-Catenin Signaling and Differentiation Potential of Bone Marrow Mesenchymal Stem Cells in Process of Bone Loss in Ovariectomized Rats. Acta Endocrinol (Buchar) 16(2):156–164
28. Wu J et al (2022) A Sonic Hedgehog-Gli-Bmi1 signaling pathway plays a critical role in p27 deficiency induced bone anabolism. Int J Biol Sci 18(3):956–969
29. Wang H et al (2023) Hippo-YAP/TAZ signaling in osteogenesis and macrophage polarization: therapeutic implications in bone defect repair. Genes Dis 10(6):2528–2539
30. Zeng L et al (2023) Ataluren prevented bone loss induced by ovariectomy and aging in mice through the BMP-SMAD signaling pathway. Biomed Pharmacother 166:115332
31. Ma S et al (2019) The Hippo pathway: biology and pathophysiology. Annu Rev Biochem 88:577–604
32. Liu Q et al (2014) E3 ubiquitin ligase Cbl-b in innate and adaptive immunity. Cell Cycle 13(12):1875–1884
33. Baird AM et al (2019) When RON MET TAM in mesothelioma: all druggable for one, and one drug for all? Front Endocrinol (Lausanne) 10:89
34. Choi WH et al (2011) Low-intensity ultrasound increased colony forming unit-fibroblasts of mesenchymal stem cells during primary culture. Tissue Eng Part C Methods 17(5):517–526
35. Shen X et al (2021) A novel circular RNA circITSN2 targets the miR-218-5p/LMO7 axis to promote chicken embryonic myoblast proliferation and differentiation. Front Cell Dev Biol 9:748844
36. Wu H et al (2017) Circulating Exosomal microRNA-96 promotes cell proliferation, migration and drug resistance by targeting LMO7. J Cell Mol Med 21(6):1228–1236
37. Dedeic Z et al (2011) Emerin inhibits Lmo7 binding to the Pax3 and myod promoters and expression of myoblast proliferation genes. J Cell Sci 124(Pt 10):1691–1702
38. Possidonio AC et al (2016) Knockdown of Lmo7 inhibits chick myogenesis. FEBS Lett 590(3):317–329
39. Levine AJ (1997) p53, the cellular gatekeeper for growth and division. Cell 88(3):323–331
40. Farr JN et al (2016) Identification of senescent cells in the bone microenvironment. J Bone Min Res 31(11):1920–1929
41. Xiang Q et al (2022) Epigenetic modifications in spinal ligament aging. Ageing Res Rev 77:101598
42. Chen W, Zhang B, Chang X (2021) Emerging roles of circular RNAs in osteoporosis. J Cell Mol Med 25(19):9089–9101
43. Zhao K et al (2018) Hsa_Circ_0001275: A potential novel diagnostic biomarker for postmenopausal osteoporosis. Cell Physiol Biochem 46(6):2508–2516
44. Zhang H et al (2021) Key circular RNAs identified in male osteoporosis patients by whole transcriptome sequencing. PeerJ 9:e11420
45. Chen Z et al (2022) Identification of circrna expression profiles in BMSCs from Glucocorticoid-Induced osteoporosis model. Stem Cells Int 2022:p3249737
46. Wang H et al (2020) Identification of circRNA-associated CeRNA network in BMSCs of OVX models for postmenopausal osteoporosis. Sci Rep 10(1):10896
47. Fu M et al (2022) Microarray analysis of circrnas sequencing profile in exosomes derived from bone marrow mesenchymal stem cells in postmenopausal osteoporosis patients. J Clin Lab Anal 36(1):e23916
48. Mi B et al (2019) CircRNA AFF4 promotes osteoblast cells proliferation and inhibits apoptosis via the Mir-7223-5p/PIK3R1 axis. Aging 11(24):11988–12001
49. Yu L, Liu Y (2019) circRNA_0016624 could sponge miR-98 to regulate BMP2 expression in postmenopausal osteoporosis. Biochem Biophys Res Commun 516(2):546–550
50. Chen X et al (2019) CircRNA_28313/miR-195a/CSF1 axis modulates osteoclast differentiation to affect OVX-induced bone absorption in mice. RNA Biol 16(9):1249–1262
51. Gao JW et al (2023) CircRBM23 regulates the switch between osteogenesis and adipogenesis of mesenchymal stem cells via sponging miR-338-3p. Clin Sci (Lond), 137(6): pp. 495–510
52. Zhi F et al (2021) Exosomal Hsa_circ_0006859 is a potential biomarker for postmenopausal osteoporosis and enhances adipogenic versus osteogenic differentiation in human bone marrow mesenchymal stem cells by sponging miR-431-5p. Stem Cell Res Ther 12(1):157
53. Huang A et al (2020) Circular RNA-protein interactions: functions, mechanisms, and identification. Theranostics 10(8):3503–3517
54. Wang Z et al (2022) Circular RNA MTCL1 promotes advanced laryngeal squamous cell carcinoma progression by inhibiting C1QBP ubiquitin degradation and mediating beta-catenin activation. Mol Cancer 21(1):92
55. Hime GR et al (1997) D-Cbl, the drosophila homologue of the c-Cbl proto-oncogene, interacts with the drosophila EGF receptor

in vivo, despite lacking C-terminal adaptor binding sites. Oncogene 14(22):2709–2719
56. Schmidt MHH, Dikic I (2005) The Cbl interactome and its functions. Nat Rev Mol Cell Biol 6(12):907–918
57. Jang HD et al (2019) C-Cbl negatively regulates TRAF6-mediated NF-κB activation by promoting K48-linked polyubiquitination of TRAF6. Cell Mol Biol Lett 24:29
58. Sévère N, Dieudonné FX, Marie PJ (2013) E3 ubiquitin ligase-mediated regulation of bone formation and tumorigenesis. Cell Death Dis 4(1):e463
59. Brennan T et al (2011) Abrogation of Cbl-PI3K interaction increases bone formation and osteoblast proliferation. Calcif Tissue Int 89(5):396–410
60. Kaabeche K et al (2004) Cbl-mediated degradation of Lyn and Fyn induced by constitutive fibroblast growth factor receptor-2 activation supports osteoblast differentiation. J Biol Chem 279(35):36259–36267
61. Kaabeche K et al (2005) Cbl-mediated ubiquitination of alpha5 integrin subunit mediates fibronectin-dependent osteoblast detachment and apoptosis induced by FGFR2 activation. J Cell Sci 118(Pt 6):1223–1232
62. Dufour C et al (2008) FGFR2-Cbl interaction in lipid rafts triggers Attenuation of PI3K/Akt signaling and osteoblast survival. Bone 42(6):1032–1039
63. Tanaka S et al (1996) c-Cbl is downstream of c-Src in a signalling pathway necessary for bone resorption. Nature 383(6600):528–531
64. Sanjay A et al (2001) Cbl associates with Pyk2 and Src to regulate Src kinase activity, alpha(v)beta(3) integrin-mediated signaling, cell adhesion, and osteoclast motility. J Cell Biol 152(1):181–195
65. Bruzzaniti A et al (2005) Dynamin forms a Src kinase-sensitive complex with Cbl and regulates podosomes and osteoclast activity. Mol Biol Cell 16(7):3301–3313
66. Moya IM, Halder G (2019) Hippo-YAP/TAZ signalling in organ regeneration and regenerative medicine. Nat Rev Mol Cell Biol 20(4):211–226
67. Pan JX et al (2018) YAP promotes osteogenesis and suppresses adipogenic differentiation by regulating β-catenin signaling. Bone Res 6:18
68. Huang S et al (2019) Loss of Super-Enhancer-Regulated circrna Nfix induces cardiac regeneration after myocardial infarction in adult mice. Circulation 139(25):2857–2876
69. Du TT et al (2019) LMO7 deficiency reveals the significance of the cuticular plate for hearing function. Nat Commun 10(1):1117
70. Holaska JM, Rais-Bahrami S, Wilson KL (2006) Lmo7 is an Emerin-binding protein that regulates the transcription of Emerin and many other muscle-relevant genes. Hum Mol Genet 15(23):3459–3472
71. Liu X et al (2021) LMO7 as an unrecognized factor promoting pancreatic cancer progression and metastasis. Front Cell Dev Biol 9:647387
72. Tzeng YW et al (2018) LMO7 exerts an effect on mitosis progression and the spindle assembly checkpoint. Int J Biochem Cell Biol 94:22–30
73. Lew DJ, Dulić V, Reed SI (1991) Isolation of three novel human Cyclins by rescue of G1 Cyclin (Cln) function in yeast. Cell 66(6):1197–1206
74. Bennett CF et al (2017) Pharmacology of antisense drugs. Annu Rev Pharmacol Toxicol 57:81–105
75. Bennett CF (2019) Therapeutic antisense oligonucleotides are coming of age. Annu Rev Med 70:307–321
76. Reilley MJ et al (2018) STAT3 antisense oligonucleotide AZD9150 in a subset of patients with heavily pretreated lymphoma: results of a phase 1b trial. J Immunother Cancer 6(1):119
77. Wang FS et al (2007) Knocking down dickkopf-1 alleviates Estrogen deficiency induction of bone loss. A histomorphological study in ovariectomized rats. Bone 40(2):485–492
78. Canalis E et al (2020) Antisense oligonucleotides targeting Notch2 ameliorate the osteopenic phenotype in a mouse model of Hajdu-Cheney syndrome. J Biol Chem 295(12):3952–3964
79. Canalis E et al (2022) Use of antisense oligonucleotides to target Notch3 in skeletal cells. PLoS ONE 17(5):e0268225
80. Wang FS et al (2011) Heat shock protein 60 protects skeletal tissue against glucocorticoid-induced bone mass loss by regulating osteoblast survival. Bone 49(5):1080–1089
81. Zhang G et al (2012) A delivery system targeting bone formation surfaces to facilitate RNAi-based anabolic therapy. Nat Med 18(2):307–314
82. Yu W et al (2023) Super enhancers targeting ZBTB16 in osteogenesis protect against osteoporosis. Bone Res 11(1):30
83. Jiang Z et al (2022) Iron overload-induced ferroptosis of osteoblasts inhibits osteogenesis and promotes osteoporosis: an in vitro and in vivo study. IUBMB Life 74(11):1052–1069
84. Shao YW et al (2020) [Mechanisms of electroacupuncture underlying treatment of osteoporosis based on HDAC2-mediated osteoblast differentiation pathway]. Zhen Ci Yan Jiu 45(6):438–445